The International Journal of Advanced Manufacturing Technology (2019) 104:1709–1731
https://doi.org/10.1007/s00170-019-03975-w

ORIGINAL ARTICLE

A review of friction stir–based processes for joining dissimilar materials

Kai Chen[1] · Xun Liu[2,3] · Jun Ni[1]

Received: 2 January 2019 / Accepted: 31 May 2019 / Published online: 14 June 2019

Abstract
This paper covers a detailed study of friction stir–related processes with the focus on joining dissimilar materials. First, the effects of the process parameters and tool geometries on weld mechanical properties, defects, and weld microstructure along with the formation and growth of intermetallics are systematically reviewed. Process-structure-property relationships are discussed in details. Second, the paper summarizes different physical models that have been developed for friction stir–related process. A specific session on modeling dissimilar material joining is provided. The objective of these models is to determine the temperature profile, stress, and strain distribution along with material flow field based on the input process parameters and tool geometries. By further implementing these results into microstructure evolution and material property models, the dissimilar material weld mechanical performance can be predicted eventually. Third, recently developed friction stir variants for process improvement and joint quality enhancement are discussed. Finally, potential future research directions are recommended in conclusion.

Keywords Friction stir–related process · Friction stir welding (FSW) · Friction stir spot welding (FSSW) · Dissimilar materials · Process parameters · Physics modeling · Innovative variants of the friction stir–related process

1 Introduction

In recent years, a growing amount of attention has been given to studies of reducing vehicle weights in the automotive industry considering both economic and environmental factors to achieve the goal. Lightweight advanced high-strength steels such as high strength low-alloy (HSLA) steel, dual phase (DP) steel, complex phase (CP) steel, transformation-induced plasticity (TRIP) steel, and interstitial-free (IF) steel are widely used in the automotive industry. Their superior properties make them excellent materials for the vehicles with the advantages of both saving weight and increasing the structural strength [1]. Among them, the DP, CP, and TRIP steels are named as the first-generation advanced high-strength steel (AHSS), which has a TS/El (tensile strength/percent elongation) ratio lower than or equal to 25,000 MPa% [2]. Regarding the TRIP steel, it contains bainite and martensite with the retained austenite in the ferrite microstructure. The existence of the retained austenite enhances the ductility of the TRIP steel by transforming the austenite to martensite during deformation. This phenomenon leads to an increase in strength, toughness, and ductility of the steel [3–7]. However, the application of the advanced high-strength steel is insufficient to meet the need of the increasingly strict emission regulations. One promising solution involves replacing steel components with multi-material vehicle structures [8]. For example, aluminum alloy is a strong candidate for partially replacing steel. However, to achieve reliable and economical dissimilar material joints is highly challenging for conventional fusion welding technologies, which rely on melting of the 2 bulk materials. First is that the base materials have extremely different physical and mechanical properties. Furthermore, the formation of a large amount of intermetallic compounds (IMCs) significantly deteriorates welding strength [9–12]. Among fusion welding processes, resistance spot welding (RSW) is the most widely used joining technique in the

✉ Xun Liu

[1] S.M. Wu Manufacturing Research Center, University of Michigan, Ann Arbor, MI 48109, USA

[2] Department of Materials Science and Engineering, The Ohio State University, Columbus, OH 43210, USA

[3] Columbus, USA

automotive industry, which shows a lot of limitations in welding aluminum to steels. First, compared with steel, the aluminum alloy has a higher thermal and electrical conductivity; the RSW process parameters include a higher current density and shorter welding time [13–16]. In the meantime, welding aluminum alloys requires an electrode force which is twice than that of welding the bare steel, which is due to its high thermal and electrical conductivity [17]. Therefore, it also brings the problems of the insistent weld quality and short electrode life [18, 19].

To overcome these challenges, friction stir welding (FSW) and friction stir spot welding (FSSW) are promising solid-state welding techniques, as the bulk melting is minimized during the process. They are considered "green" technologies based on their high energy efficiency. Different from the conventional fusion welding methods, neither shielding gas nor consumable materials are needed [20].

1.1 Friction stir welding

Friction stir welding was introduced and patented by The Welding Institute (TWI) in 1991, which has mainly been applied to weld aluminum alloys [21]. Applications of FSW have then extended to the magnesium, conventional steel, AHSS, and even polyethylene. Furthermore, both the similar material welding and dissimilar material welding are investigated by the researchers [22–24]. During FSW, a rotating tool with a cylindrical pin feature is gradually plunged into the welding materials with a prescribed speed until the desired plunge depth is reached. The tool is then held rotating for a short period of dwell time. After that, the tool moves along the joint line under a certain prescribed travel speed. Finally, the tool is retracted at the final position and the weld is achieved. The side where the direction of the rotation tool is the same as the traverse direction is referred to as the advancing side while the other is the retreating side [25]. The welding process and the corresponding setup are illustrated in Fig. 1 [20]. FSW is widely used in both the butt joint and lap joint configurations. The joint performance highly depends on the tool offset, welding speed, rotational speed, weld pitch (ratio of the welding speed to the rotational speed), plunge depth/forging force, and the tool geometry. It was reported from Seidel and Reynolds [26] that the weld pitch is inversely correlated with the specific weld energy, which is the energy input per unit weld length. Balasubramanian [27] studied effects of the weld pitch for different aluminum alloys. Higher weld pitch would lead to a lower YS and hardness. A higher weld pitch introduces insufficient heat input in the welding zone, which reduces the material flow around the tool pin and deteriorates the final joint quality.

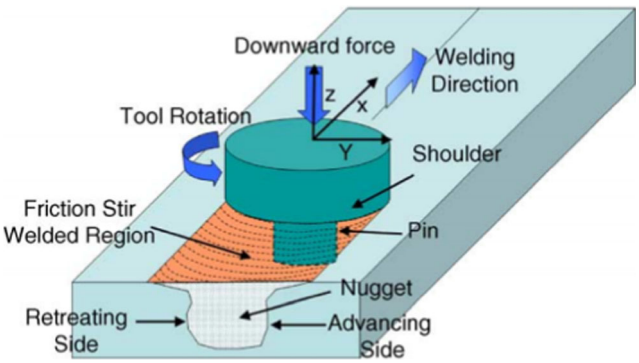

Fig. 1 Illustration of the friction stir welding process [20]

1.2 Friction stir spot welding

Friction stir spot welding is a variation of FSW, which is introduced by the US patent 6,601,751 B2 [28]. Instead of the moving the rotating tool along the butt line, a spot joint is made where the welding tool penetrates the top sheet and holds rotating for a short period (dwell time) to make the joint. A schematic illustration of the welding process is shown in Fig. 2. The joint strength of the FSSW is affected by the process parameters, which includes the rotation speed, the plunge speed, the plunge depth, and the dwell time. Besides, the tool geometries also play an important role in determining the heat generation, material flow, and accordingly joint performance. A considerate amount of studies has been conducted on the FSSW of aluminum alloys, including aluminum alloys 5052 [30, 31], 5083 [8], 5754 [32, 33], 6061 [34–39], 6011 [40], 7050 [41] and 7075 [42]. In addition, increasing interests in the dissimilar material welding brings the attention to the FSSW, especially for the aluminum alloy to the conventional steel, which includes the welding of aluminum alloy 6016 to IF steel [43], 6061 to low-carbon steel [44], 6061 to AISI 1018 [45], 6111 to DC04 steel [46], 1050 to hot-stamped boron steel [47], and 5083 to St-12 steel [48].

Applications of FSSW are growing in the automotive industry. However, there are still some disadvantages of the FSSW process, among which the keyhole that is left after the retraction of the welding tool at the end of the welding process is a major issue. The keyhole can lead to a large amount of stress concentration under external loading. It is also difficult for the body paint to reach the keyhole bottom, which results in potential corrosion issues [49]. To refill the keyhole after the welding process, a novel keyhole refilled FSSW method is developed, which was first described in US Patent 6,722,556 B2 [50]. The process contains the following steps: In the first step, the clamping ring moves downward and presses the base material against the anvil at the bottom. In the second step, the sleeve rotates and plunges into the base material while the tool pin moves upward simultaneously. The frictional heat from the rotating sleeve plasticizes the workpiece materials and enables them to occupy the available space formed between the pin and sleeve. In the third step, the sleeve moves upward and the pin moves downward,

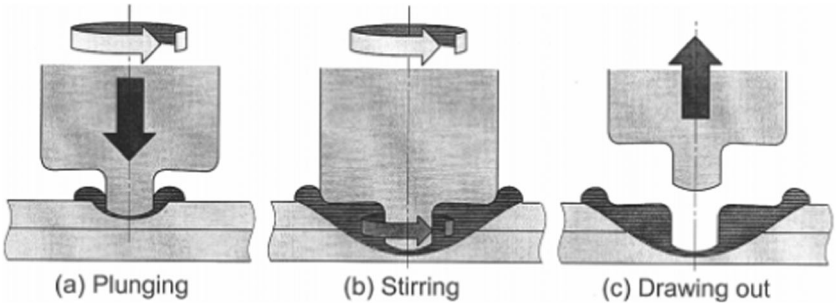

Fig. 2 Illustration of the FSSW process [29]

which pushes the accumulated material back to fill the keyhole. In the final step, the entire welding tool retracts without a keyhole left on the surface. The entire process is illustrated in Fig. 3. It has been applied in joining aluminum alloy [49, 51, 52] and dissimilar materials [53–55].

This paper covers the experimental and model analysis on FSW and FSSW processes for joining dissimilar materials. Effects of welding parameters and tool geometries on the microstructure and corresponding joint strength are comprehensively reviewed. More attention will be paid on the IMC formation and weld defect generation. Then, analytical and computational models of FSW and FSSW processes, microstructure evolution, and weld property models are discussed, which forms the basis of integrated computational materials engineering (ICME) in friction stir–related dissimilar material joining process. The rest of the paper discussed several novel improvements of the friction stir–related process. Finally, a summary is given and future research directions are proposed.

2 Experimental studies

Abundant researches have been conducted on FSW and FSSW of various pairs of dissimilar materials with focuses on the process-structure-property relationships. The change of the process conditions has an important impact on the material flow and the IMC formation of the welding zone, which are determining factors for the joint quality. The following sections discussed experimental studies for different solid-state welding processes, including the FSW, friction stir lap welding, FSSW, and keyhole refilled FSSW.

2.1 Friction stir welding

During the dissimilar FSW process, as the base materials have different chemical and mechanical properties from each other, the tool offset becomes a critical parameter for determining the joint quality. For FSW of dissimilar materials, generally, the tool shifts at a certain distance from the original butt line and towards the soft material side. This distance is defined as the tool offset, which is a critical parameter on the final joint quality. Tool offset determines the material distribution in the weld, which affect the IMC formation at the interface of the dissimilar materials. Sahu et al. [56] studied the effect of the tool offset on dissimilar FSW of 1050Al and pure Cu with the thickness of 4 mm, where Cu has a higher yield strength and hardness. A cylindrical pin tool is used, with the tool shoulder diameter of 25 mm, pin diameter of 6 mm, and pin length of 3.5 mm. A tool offset less than 1.5 mm towards the Al side results in defects in the welding zone with inappreciable joint strength. It was also found that the flow of the IMCs was discontinuous and non-uniform in the NZ. Different from the previous conditions, when the tool offset reached 1.5 mm, a thin and uniform continuous IMCs were formed at the NZ and the resulting tensile test showed a better UTS and YS. Regarding the grain size in the NZ, the average value for Al is 63.32 μm and for Cu is 55.45 μm under the tool offset of 1.0 mm. As the tool offset increases to 1.5 mm, the grain size of Al and Cu reduces to 44.18 μm and 42.92 μm respectively. Liu et al. [57] studied FSW of TRIP 780/800 steel to aluminum alloy 6061 with the thickness of 1.4 mm and 1.5 mm. A conical pin tool is used, with the shoulder diameter of 12.7 mm and pin length of 1.2 mm. The tool offset was considered in their experimental work, which was set as 1.03 mm

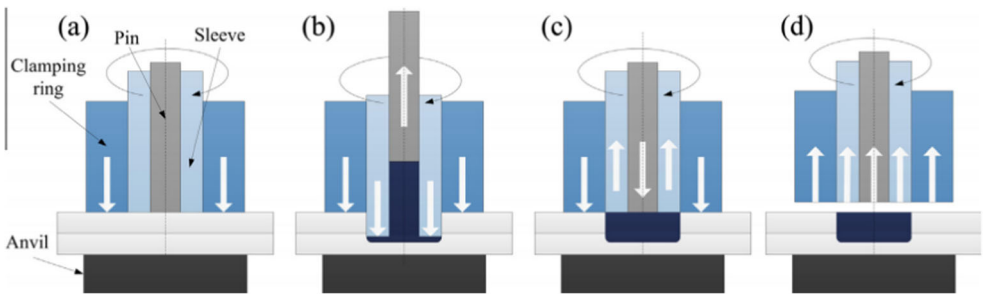

Fig. 3 Schematic illustration of the refilled friction stir spot welding process [51]

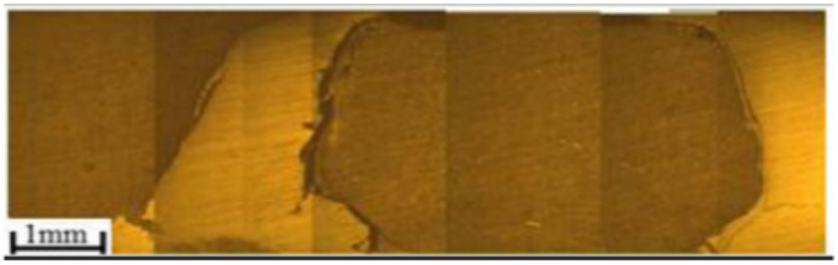

Fig. 4 A continuous chunk of steel is separated from the steel side and cracks are generated surrounding the chunk [58]

and 1.63 mm away from the butt line towards the aluminum side. Analyzing the microstructure of the welding cross section indicated that an interlayer was formed at the Al-Fe interface. With the tool offset of 1.03 mm, a thicker interlayer was generated when compared with the 1.63-mm tool offset. It can be explained by the measured temperature data. As the tool offset was at 1.03 mm, a higher peak temperature was observed at different locations of the aluminum sheet, which enhanced the atom diffusion rate at the Al-Fe interface and resulted in a thicker interlayer. In the meantime, a higher peak temperature resulted in a lower vertical force and lateral force during the welding process. The authors mentioned that a joint with a thin continuous IMC layer would provide a higher tensile strength compared with the joint without the IMC layer. Habibnia et al. [58] investigated the FSW of aluminum alloy 5050 to 304 stainless steel plates with 3 mm thickness. Their tool has a shoulder diameter of 20 mm and pin length of 2.75 mm. The offset of the welding tool was set up as 0 mm, 0.8 mm, and 1.5 mm away from the butt line towards the aluminum side. The authors mentioned that a larger tool offset achieved a defect-free surface finish. Furthermore, the microstructure images showed that a continuous layer of steel was separated from the steel side if the tool is placed in the center, which caused cracking as shown in Fig. 4. After the tool offset increased to 0.8 mm, the formation of the tunnel was found at the welding nugget, which was also undesirable. For the tool offset of 1.5 mm, small steel particles were found in the stir zone and the highest tensile shear strength was obtained. The defects generated at the welding surface and the welding zone were mainly due to the lack of sufficient material flow during the welding process. As the aluminum alloy has a lower melting temperature and yield strength compared with steel, it has a better material flowability under the same temperature. As the tool offset changes from 0 to 1.5 mm, less steel was involved in the welding process, which made it easier for the tool to drive the material around the tool pin and result in a better material mixing and joint strength. Xue et al. [59] studied the effect of the pin offset by welding the 1060 aluminum alloy and commercial pure copper with 5 mm thickness. A conventional tool was used in their experimental work, with the tool shoulder diameter of 20 mm, pin diameter of 6 mm, and pin length of 4.8 mm. A good surface morphology was obtained when the pin offset was equal to or larger than 2 mm towards aluminum. The authors mentioned that when the tool offset was relatively large, only a few Cu pieces were scratched from the Cu bulk, which made it easier to mix with the Al base. In this case, a sound metallurgical bonding was obtained. Fu et al. [60] performed friction stir welding between aluminum alloy 6061-T6 and Mg alloy AZ31B-O. Both of the materials have a thickness of 3 mm. A conventional tool was used, with the tool shoulder diameter of 10 mm, pin diameter of 3.2 mm, and pin length of 2.8 mm. The highest tensile strength was obtained when the Mg was placed in the AS side and the tool offset was set to 0.3 mm towards Mg.

2.2 Friction stir lap welding

As a variant of friction stir welding, friction stir lap welding (FSLW) focuses on the lap welding configuration. During

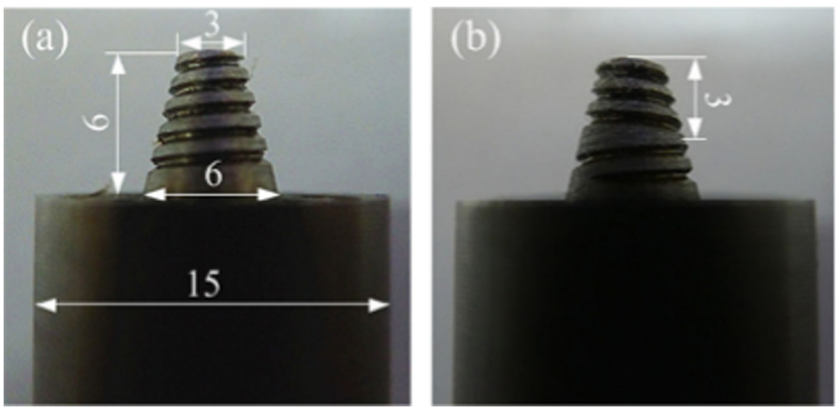

Fig. 5 Illustration of the threaded and reverse-threaded tool pin features [61]

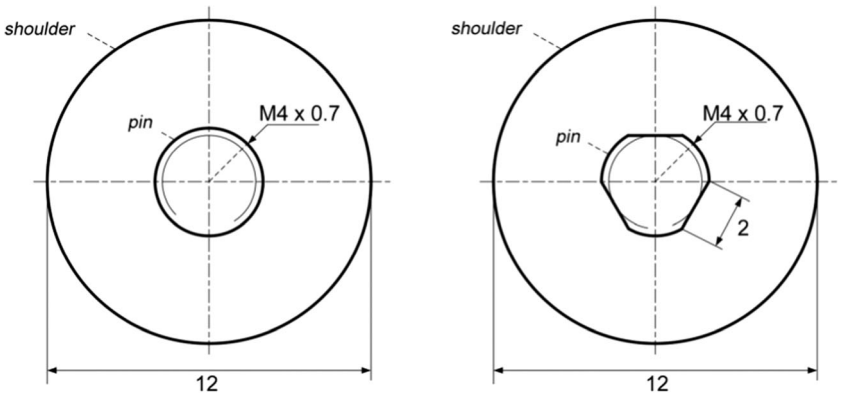

Fig. 6 Schematic illustration of the welding tool geometries [63]

FSLW, the tool shoulder touches the surface of the top metal and the rotating tool pin inserts into both sheets to make a joint, the geometry of the tool pin is crucial to the final welding quality. Yue et al. [61] studied the effect of the reverse-threaded pin on the mechanical properties for FSLW of the aluminum alloy 2024. In their experimental studies, one of the tool pins was fully threaded and the other had the reversed thread from the middle to the tip of the pin, which is shown in Fig. 5. By applying both tools in the welding process, the cross-sectional view indicated that the reverse thread pin has a larger lap width, which was defined as the width of the bonding area from AS to RS. It was explained as a result of the upward flow motion of the welding material driven by the reverse-threaded tool pin. Regarding the grain structure, the threaded pin pushed the material to the bottom side and the resistance force was generated from the TMAZ. While the reverse-threaded tool pin pushed the material upward, which led to a higher flow rate and larger strain. Thus, a better grain structure was observed from the microstructure in the NZ. Ge et al. [62] investigated the effect of tool pin length for FSLW of aluminum alloy 7075 and aluminum alloy 2024. The thickness of both is 3 mm. The plunge depth was 0.2 mm in their study, which was defined as the distance between the shoulder surface and the top metal sheet. The applied tool pin had the length of 3 mm, 4 mm, and 5 mm. From the microstructure of the cross-sectional view, the 3-mm tool only touched a small portion of the lower sheet, which resulted in a smaller bending degree of the hook and lowest welding strength. Four-millimeter and 5-mm tool pins increase the hook bending degree and height and joint strength. The longer welding tool pin ensures sufficient stirring action, which enhances the material flow on the bottom sheet. Balakrishnan et al. [63] studied the influence of tool wear on the tensile and fatigue behavior of the FSLW with AA 7075-T6. Two welding tools were applied, one with a threaded cylindrical pin and the other was a cylindrical tool pin with some flats, as shown in Fig. 6. The flats in the tool pin are to simulate the tool wear and material adhesion to the tool. It was reported that the change of the tool geometry had no effect on the peak temperature during the welding process, which indicates that the change of the joint properties was mainly attributed to the difference of the material flow driven by the tool. No influence on the bonded interface width (BIW) was found from the two welding tools. The tool with the flat machines tool pin increases 10% in the effective sheet thickness (EST), which contributed to a 500% increase in the fatigue life. The measurements of the BIW and EST are defined in Fig. 7. Saeid et al. [64] investigated friction stir lap welding of 1060 aluminum alloy and commercial pure copper. Their maximum tensile strength is achieved at welding speed of 95 mm/min and tool rotational speed of 1180 rpm. It was found that a smaller welding speed than this value would reduce the joint strength due to the increasing volume of copper particles in the welding interface. In the meantime, a higher welding speed was also not desirable as it generated incomplete welded interfaces with occurrences of cavities. Chen et al. [65] studied tool geometry effects on friction stir lap welding of AZ31 magnesium alloy to steel. The results showed that the joint strength was positively correlated with the probe length. However, the result is different when the Zn-coated steel was applied.

2.3 Friction stir spot welding

As a variation of the friction stir welding process, friction stir spot welding (FSSW) is applied for a spot weld configuration. Process parameters for FSSW include the rotation rate, plunge speed, dwell time, and plunge depth, which is defined as the distance between the surface of the top sheet to the tip of the

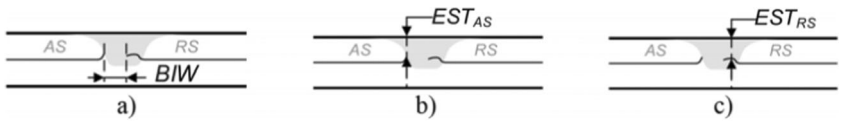

Fig. 7 Measurement of the BIW and EST for the friction stir lap welding [63]

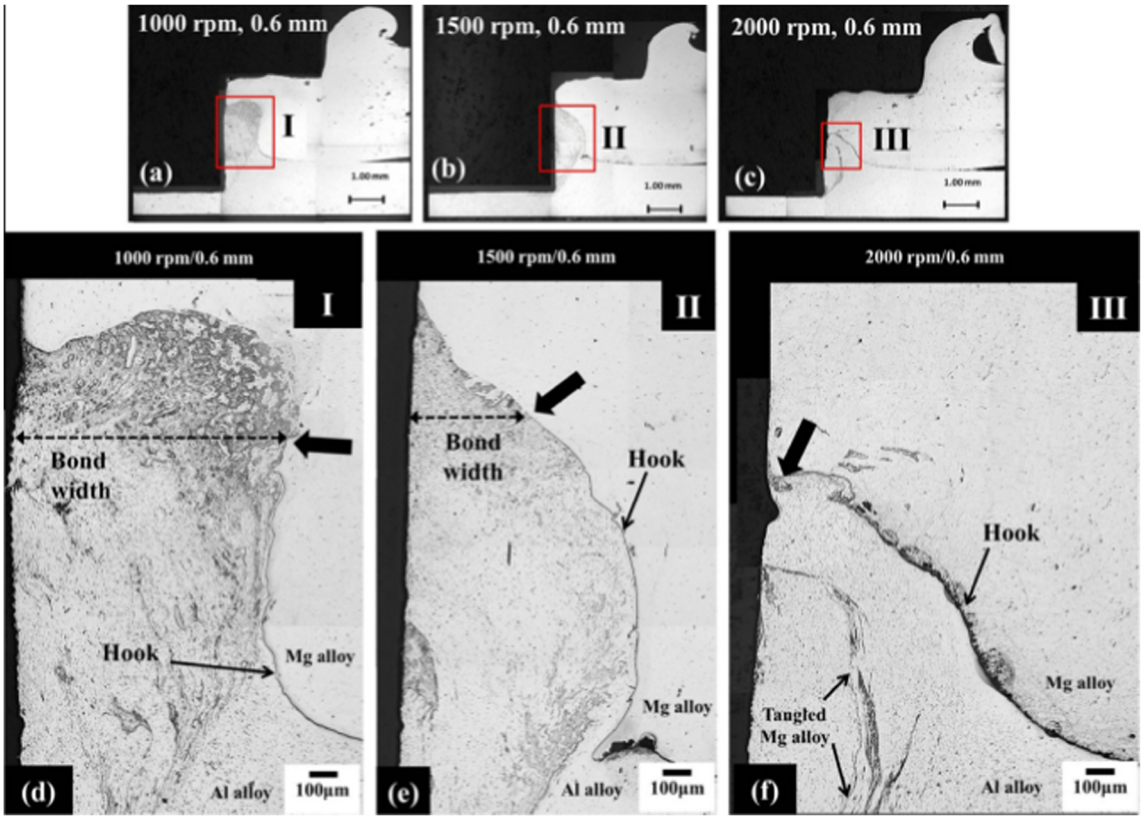

Fig. 8 Illustration of the bond width at different welding speeds [22]

tool pin. Rao et al. [22] investigated the effect of the process parameters for the FSSW of magnesium to aluminum alloys. Weld microstructure on the cross section showed that a higher rotation speed resulted in a smaller bond width. The bond width is defined as the distance from the tip of the hook to the key-hole interface, as indicated in Fig. 8. As higher rotation speed increases the heat generation rate, the viscosity of the material around the welding tool pin is decreased and driving force from the tool pin was also reduced. The smaller bond width corresponds to a lower joint strength. Accordingly, a higher rotating speed reduces the joint strength. The plunge depth shows a positive correlation with the stir zone and the bond width. At a higher plunge depth, larger amount of Al is extruded from the bottom and mixed with Mg. Lee et al. [66] performed FSSW of aluminum alloy (thickness 1 mm) to the low-carbon steel (thickness 0.6 mm). An IMC layer with the thickness of 2 μm was formed at the interface. Area of the IMC increased with the tool penetration depth. Thickness of the IMC is considered to depend on the dwell time. Fereiduni et al. [48] also reported that after reducing the rotational speed from 1100 to 900 rpm, the IMC layer thickness can still increase from 2.3 to 2.9 μm through increasing the dwell time from 10 to 15 s. Since a longer dwell period results in more time for diffusion at high temperature, nucleation and especially growth of IMC are enhanced. Accordingly, higher amount of IMC can be generated. Bozzi et al. [43] did FSSW on 1.2-mm Al 6061 to 2.0-mm IF steel. The authors found out that the amount of IMC increased with the rotational velocity and penetration depth. They reported an optimal IMC layer thickness for a strong joint was 8 μm. Chowdhury et al. [67] made FSSW welds for 2.0-mm AZ31B-H24 Mg and Al5754. The existence of IMC $Al_{12}Mg_{17}$ and Al_3Mg_2 was identified by XRD analysis and it resulted in a high hardness of HV 125, which created an easy fracture path during the tensile test. The authors also mentioned that restraining IMC formation by using an adhesive was beneficial to the joint strength. Sato et al. [68] applied friction stir spot welding to 1.2-mm AA5083 with 1.3-mm AZ31. It was mentioned that the tensile strength reduced significantly when the IMC was thicker than 1.8 μm. They mentioned that there was no obvious dependence between IMC thickness and the lap shear tensile strength. However, the fracture surface showed that the brittle IMC provides an easy fracture path. Table 1 summarizes the investigated dissimilar FSSW conditions and corresponding joint strength in previous literature.

Besides the welding process parameters, the geometry of the welding tool is another important factor in determining the joint quality. Piccini and Hernan [74] studied the effects of the pin length for FSSW of aluminum alloy 6063 (thickness 2 mm) to galvanized low-carbon steel (thickness 0.7 mm). Three tool pin lengths were applied, including 1.5 mm,

Table 1 Comparison of the lap shear strength for dissimilar material FSSW welds

Base material	Thickness	Maximum lap shear force (kN)	Optimized process parameters
Aluminum alloy 5052 C1100 copper alloy [69]	1 mm, 1 mm	0.8	Rotation speed: 3500 rpm Plunge speed: 6 mm/min Dwell time: 4 s Plunge depth: 1.7 mm
Aluminum alloy 6022 Magnesium alloy AM608 [22]	1.5 mm, 3.1 mm	2.5	Rotation speed: 1000 rpm Plunge speed: 12 mm/min Dwell time: 1 s Plunge depth: 4.4 mm
Aluminum alloy 5083 Magnesium alloy AZ31 [68]	1.2 mm, 1.3 mm	2.1	Rotation speed: 2250 rpm Plunge speed: 5 mm/min Dwell time: 2 s Plunge depth: 1.9 mm
Aluminum alloy 5754 Magnesium alloy AZ31 [67]	2.0 mm, 2.0 mm	1.3	Rotation speed: 2000 rpm Plunge speed: 3 mm/min Dwell time: 2 s Plunge depth: 3.0 mm
Aluminum alloy 1100 SGACD zinc-coated steel [70]	1.0 mm, 1.0 mm	1.9	Rotation speed: 4000 rpm Plunge speed: 6 mm/min Dwell time: 6 s Plunge depth: 1.0 mm
Aluminum alloy 6016 IF steel [43]	1.2 mm, 2.0 mm	4.5	Rotation speed: 3000 rpm Plunge depth: 2.9 mm
Aluminum alloy 6061 Mild steel [71]	1.0 mm, 1.0 mm	3.6	Rotation speed: 700 rpm Apply load: 500 kg Plunge depth: 2 mm
Aluminum alloy 5754 HX 340LAD steel [72]	2.0 mm, 1.0 mm	6.5	Rotation speed: 2400 rpm Plunge speed: 12 mm/min Dwell time: 3 s Plunge depth: 2.2 mm
TRIP 780 steel HSBS steel [73]	1.5 mm, 1.4 mm	13.3	Rotation speed: 800 rpm Plunge speed: 0.3 mm/min Dwell time: 8 s Plunge depth: 2.5 mm
Aluminum alloy 6061 TRIP 780 steel [23]	1.5 mm, 1.5 mm	4.1	Rotation speed: 2000 rpm Plunge speed: 10 mm/min Dwell time: 5 s Plunge depth: 1.9 mm

1.0 mm, and 0.5 mm. To evaluate the effect of pin length independently, the distance between the tip of the tool pin and the bottom sheet was kept constant during all the tests. The authors mentioned that a shorter tool pin could enhance the joint strength since the shoulder plunge depth is higher. This increased the heat generation rate at the tool shoulder and improved material flow of the aluminum alloy. Accordingly, the bonding is enhanced between the welding materials. Lin and Chen [75] studied the effects of different thread locations for FSSW of aluminum alloys. They were named B-Tool, M-Tool, and T-tool, which are shown in Fig. 9. Weld cross sections show that more materials were mixed when applying the B-tool, as in Fig. 10. This was due to the location of the thread in the B-Tool was nearest to the tool shoulder, which drove a larger amount of the upper sheet materials to flow downward. It was also found that the stir zone shifted downward together with different locations of the thread on the tool pin, which indicated the stir zone was enlarged with the thread feature.

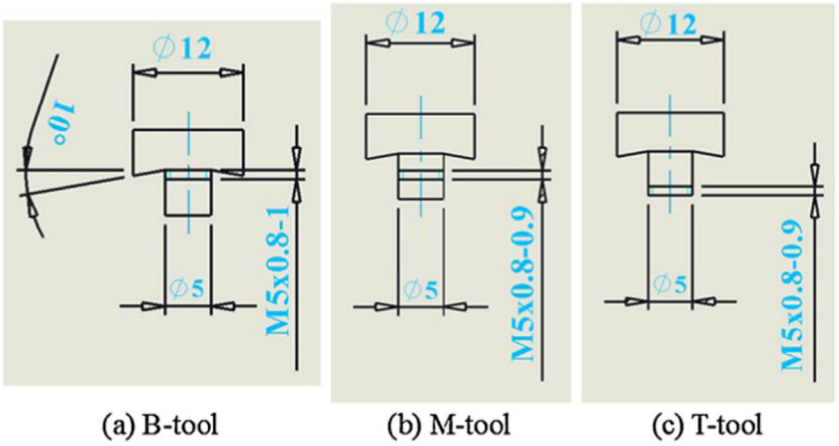

Fig. 9 Illustration of different thread locations in the tool pin [75]

2.4 Refill friction stir spot welding

The refill friction stir spot welding attracts more and more attention these days with its advantages of removing the keyhole immediately after the process. Refill FSSW has a different welding tools and working mechanism scompared with the conventional FSSW and correspondingly the critical process parameters are different. Shen et al. [76] applied different tool designs for the refill FSSW of aluminum alloy 6022 to aluminum alloy 7075. The welding tool sleeve was modified with three equal distributed trapezoidal grooves machined at the sleeve bottom, as shown in Fig. 11. The authors mentioned that these grooves on the sleeve increased the interaction surface area between the material and the tool, which enhanced the material flow and achieved a better metallurgical bonding. Suhuddin et al. [77] performed refill FSSW to join AA5754 Al to AZ31 Mg alloys. The presence of the IMCs at the interface played an important role in determining the mechanical properties of the joint. The distribution of the IMCs closely depends on the tool movement. On the other hand, studies on refill FSSW of aluminum alloy to steel are limited. Dong et al. [78] investigated refill FSSW of Aleris Superlite 200 ST aluminum alloy (thickness 1.5 mm) to the ST06 Z galvanized steel sheet (thickness 1.2 mm). In their experiments, the

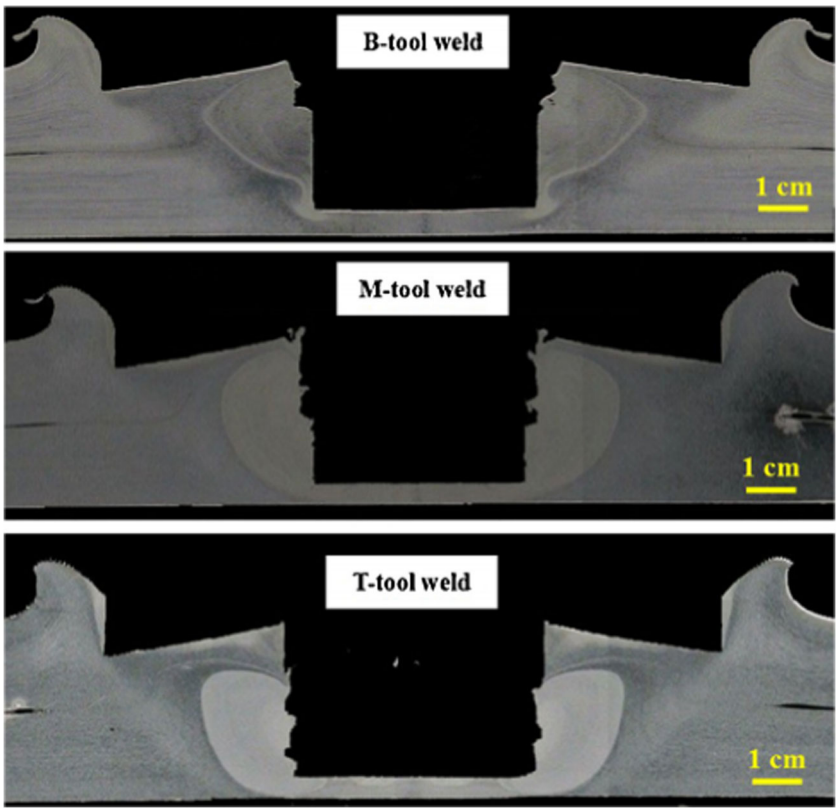

Fig. 10 Cross-sectional view of the stir zone with different tool pin thread locations [75]

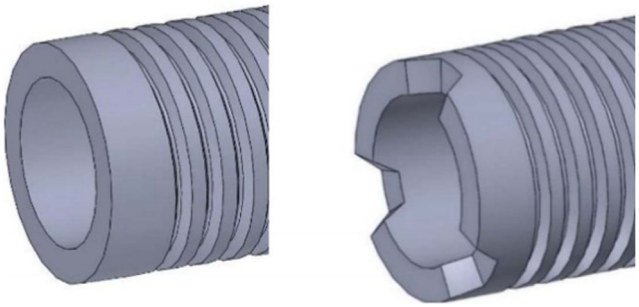

Fig. 11 Illustration of the regular tool sleeve and the modified tool sleeve [76]

plunge depth of the sleeve changed from 0.9 to 1.6 mm. It is found that the tensile/shear fracture load increased with a higher plunge depth. A maximum joint strength of 4.5 kN is achieved. In the meantime, the ZnO was found in fracture surfaces on both aluminum alloy and steel side, indicating ZnO is the weakest location of RFSSW weld. One issue with RFSSW is the tendency of the plasticized material sticking between the separately moving pins and shoulders during the welding process. Shen et al. [54] performed dissimilar refill friction stir spot welds between ZEK 100 Mg alloy and galvanized DP600 steel. The tool comprises a clamping ring, sleeve, and a pin with the diameters of 15, 9, and 6.4 mm respectively. They reported that acceptable welds can be achieved when the sleeve is plunged to a depth of 0.05 mm above the Mg/steel interface without contacting the DP600 steel. Zn coating on the steel contributes to brazing outside of the weld boundary and promotes bond formation. Chen et al. [53] did a similar study but with different tool dimensions, where the pin and shoulder diameters are 6.3 mm and 10 mm respectively. Their tool rotational speed varies from 1600 to 2100 rpm, welding time varies from 2.5–3.5 mm, and sleeve plunge depth varies from 1.3 to 1.5 mm. A continuous layer of $FeAl_2$ particles is observed at the Mg/steel interface, which is hypothesized to originate from the galvanized coating on steel. Suhuddin et al. [79] welded an Al-Mg-Mn aluminum alloy to a zinc-coated HSLA steel. At the Al-Fe interface, there is a Zn-rich aluminum layer near the aluminum side and an intermetallic layer of Fe_2Al_5 and Fe_4Al_{13} near the steel side. A "stop action" weld was also made to better understand the microstructure evolution, where the process was interrupted during the tool dwell stage and quenched to room temperature. A Mg-Al-rich Zn liquid was revealed, which was proposed as the initiating phase to form the Al solid structure islands and Al-Fe intermetallic at the interface. Ding et al. [80] applied refill FSSW to join aluminum alloy AA5754 to hot-dipped AlSi-coated high-strength Usibor 1500P steel. Joint strength increases with the plunge depth. However, the plunge depth should always be smaller than the thickness of the top aluminum sheet to avoid severe wear of the sleeve as it touches the bottom steel. The AlSi coating on the original steel sheet consists of two intermetallic phases, among which the Al_7Fe_2Si plays a critical role in welding while the $Al_5Fe_2(Si)$ effectively restrains additional IMC formation and growth. Fukada et al. [81] performed refill FSSW on Al6061 to zinc-coated low-carbon steel. With appropriate plunge depth, button pullout failure mode was achieved on the welds during lap shear tensile tests. All their specimens were fractured in aluminum sheet. Table 2 summarizes the studies on refill FSSW, where the achieved maximum joint strength and corresponding welding parameters are provided.

3 Physical modeling of friction stir–related process

Current FSW models focus primarily on joining similar materials and can generally be categorized into three types: thermal models, thermal-mechanical models based on solid mechanics, and thermal-mechanical models based on fluid dynamics. In thermal modeling works, various methods have been developed to calculate the heat source at the tool-workpiece interface for prediction of the temperature profile [89–93]. Khandkar et al. [89] built up a model under a uniform shear stress distribution assumption and calculated the heat generation rate based on the measured torque and machine power. The model was implemented through the commercially available software Abaqus. Inverse analysis is applied to determine the heat input and other thermal parameters, including heat transfer coefficient between the welding materials and fixture [92, 94, 95] and heat partition between tool and workpiece [91]. The calculated temperature history can be applied to predict residual stress [96] and analyze the additional decoupled thermal-mechanical properties [92, 97].

To further understand the process, including material flow, stress, and strain distribution, fully coupled thermal-mechanical models need to be developed. Modeling challenges exist in three aspects: First, during the welding process, large amount of material deformation is involved, which leads to element distortions and numerical instabilities. Second, the accuracy of constitutive material models at high temperature, high strain, and strain rate is insufficient [98]. Third, the mechanical and thermal interaction properties between the welding tool and workpiece along with workpiece and backing plate are difficult to determine, particularly the frictional behavior [99, 100].

3.1 Solid mechanics approach

One group of the coupled thermal-mechanical models is based on solid mechanics theories under Lagrangian formulation, which enables the simulation of the entire FSW process, including plunge, dwell and welding stages. Trimble et al. [101] developed a finite element model based on a finite element package DEFORM 3D to predict the welding forces and the

Table 2 Comparisons of the maximum lap shear force from refilled FSSW

Base material	Thickness	Maximum lap shear force	Process parameter
Aluminum alloy 7B07 [51]	1.9 mm	11.9 kN	Rotation speed: 1500 rpm Plunge speed: 1 mm/s Plunge depth: 3 mm
Aluminum alloy 6061 [82]	4.8 mm	331 MPa	Rotation speed: 2290 rpm Plunge speed: 1.93 mm/s Clamping force: 16 kN
Aluminum alloy 6061 [83]	2.0 mm	143 MPa	Rotation speed: 1500 rpm Plunge depth: 2.1 mm Joint time: 2 s
Aluminum alloy 6181 [84]	1.7 mm	6.8 kN	Rotation speed: 2400 rpm Plunge depth: 1.75 mm Joint time: 3 s
PMMA cast plaques [85]	3.0 mm	9.5 MPa	Rotation speed: 500 rpm Plunge speed: 1.75 mm/min Joint pressure: 3 bar Plunge depth: 4 mm
Aluminum alloy 5042 [86]	1.5 mm	6.3 kN	Rotation speed: 900 rpm Plunge speed: 1.52 mm/min Plunge depth: 1.55 mm Plunge time: 1.02 s
Aluminum alloy 5754 and magnesium AZ31 [77]	2.0 mm	3.7 kN	Rotation speed: 1900 rpm Plunge depth: 1.8 mm Swell time: 2 s Clamping force: 12kN
Magnesium AZ31 [87]	2.0 mm	4.84 kN	Rotation speed: 1500 rpm Plunge depth: 2.75 mm Dwell time: 1 s
Aluminum alloy 2024 [88]	1.5 mm (top) 2.0 mm (bottom)	9.2 kN	Rotation speed: 1000 rpm Plunge depth: 1.8 mm Dwell time: 2 s Dwell speed: 800 rpm
Magnesium alloy ZEK100 and galvanized DP600 steel [53]	1.53 mm,1.0 mm	4.7 kN (maximum)	Rotation speed: 1800 rpm Plunge depth: 1.5 mm Dwell time: 3 s
Magnesium alloy ZEK100 and galvanized DP600 steel [54]	1.5 mm (Mg—top) 0.9 mm (steel—bottom)	3.62 kN	Rotation speed: 1800 rpm Plunge depth: 1.45 mm Dwell time: 3 s
Al-Mg-Mn aluminum alloy and hot-dip-galvanized HSLA steel [79]	3 mm (Al—top) 2 mm (steel—bottom)	7.8 kN	Rotation speed: 1600 rpm Plunge depth: 2.8 mm Dwell time: 4 s Sleeve plunging/retracting rate: 1.4 mm/s
AA5754 and Usibor 1500P steel [80]	1.6 mm (Al—top) 2 mm (steel—bottom)	4.2 kN	Rotation speed: 2000 rpm Plunge depth: 2.8 mm Dwell time: 1.5 s Plunge time: 1.5 s Refill time: 0.5 s
A6061-T6 and hot-dip zinc-coated carbon steel [81]	1.0 mm (Al—top) 1.2 mm (steel—bottom)	3.5 kN	Rotation speed: 1600 rpm Plunge depth: 0.85 mm Plunge force: 8.5 kN
Aleris Superlite 200 ST aluminum alloy and ST06 Z galvanized steel [78]	1.5 mm (Al—top) 1.2 mm (steel—bottom)	4.5 kN	Rotation speed: 2800 rpm Plunge depth: 1.6 mm Dwell time: 3.0 s Clamping force: 12 kN Refill time: 1.0 s

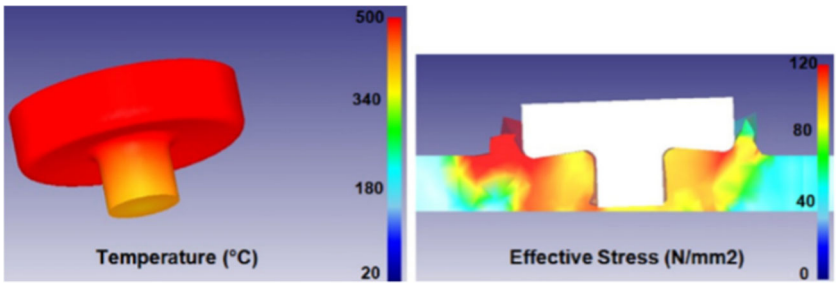

Fig. 12 FEM temperature and stress profile during the translation stage [101]

temperature profile during FSW of Al 2024 plates. The two aluminum sheets were modeled as a continuous block to avoid numerical contact instabilities. From the numerical analysis, a significantly higher stress and temperature distribution were found on the tool shoulder during the translation stage, as shown in Fig. 12. It was also shown that the threaded pin resulted in a larger material deformation volume than the smooth pin design, as provided in Fig. 13.

Yu et al. [102] applied the Johnson-Cook material failure model into ABAQUS/Explicit to dynamically remove the severely distorted elements. Their results showed that the peak temperature transferred from the region beneath the pin to the corner between pin and shoulder during the plunge stage. In the meantime, the authors mentioned that the temperature was symmetrically distributed and presented as a V shape, as shown in Fig. 14.

Mandal et al. [103] adopted ABAQUS/Explicit to model the plunge stage of FSW for Al 2024. The arbitrary Lagrangian-Eulerian (ALE) dynamic remeshing algorithm is utilized to maintain the mesh integrity during the process and avoids potential numerical divergence. The Johnson-Cook material law was adopted, as provided in Eqs. 1 and 2, where $\bar{\varepsilon}_{pl}$ is the effective plastic strain, $\dot{\bar{\varepsilon}}_{pl}$ is the effective plastic strain rate, $\dot{\varepsilon}_0$ is the normalizing strain rate and its value is commonly chosen as 1 s^{-1}, T_{melt} and T_{ref} are material melting temperature and reference temperature with the value of 20 °C, A, B, C, n', and m' are material constants. Their calculated temperature profile showed a good correlation with the experimental data for the first 5 s.

$$\sigma_e = \left(A + B\bar{\varepsilon}_{pl}^{n'}\right)\left(1 + C\ln\frac{\dot{\bar{\varepsilon}}_{pl}}{\dot{\varepsilon}_0}\right)\left(1-\hat{T}^{m'}\right) \quad (1)$$

$$\hat{T}^{m'} = \begin{cases} 0 & T < T_{ref} \\ \dfrac{T-T_{ref}}{T_{melt}-T_{ref}} & for \quad T_{ref} \le T \le T_{melt} \\ 1 & T > T_{melt} \end{cases} \quad (2)$$

Similarly, Schmidt et al. [104] applied ALE remeshing technique and the Johnson-Cook material law in ABAQUS to model FSW of Al 2024. Their model was capable of predicting the void formation during the welding process, as shown in Fig. 15.

Guerdoux et al. [105] implemented automatic remeshing in the 3D Forge3 FE software and adaptive ALE formulation to compute the material flow and temperature profile during FSW process. The Hansel-Spittel constitutive equations were utilized as the constitutive material model and the friction behavior between the tool and plate was governed by the Norton law. Their calculated welding force, welding temperature, and welding torque agreed well with the experimental data. The model was also capable of reproducing macroscopic features in the welding process, including formation of voids, influence of the threads on the material flow, and the contact zones. Jedrasiak et al. [106] presented a finite element thermal model for FSSW of Al 6111 and DC04 steel with Abaqus. In their model, the temperature was successfully predicted in a range of process conditions and the developed model was also used to predict the growth of the IMCs in the aluminum steel interface. The 1D growth rate of IMC along the direction

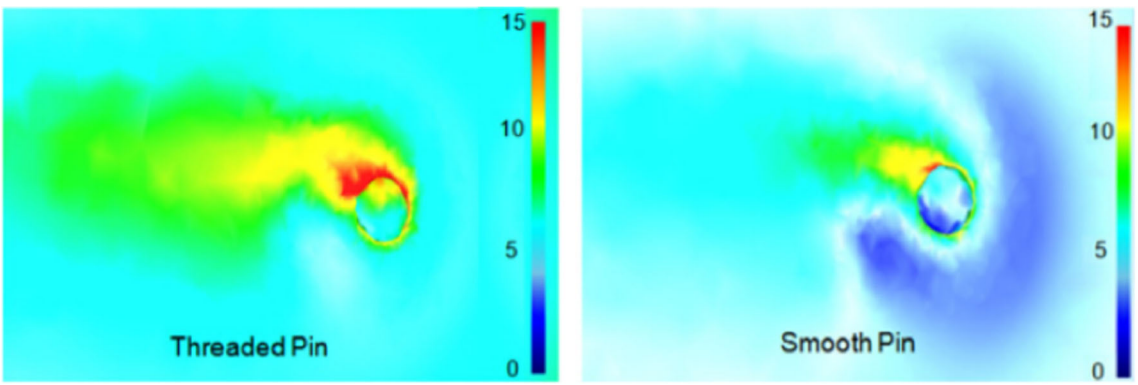

Fig. 13 Material displacement for different tool pin designs [101]

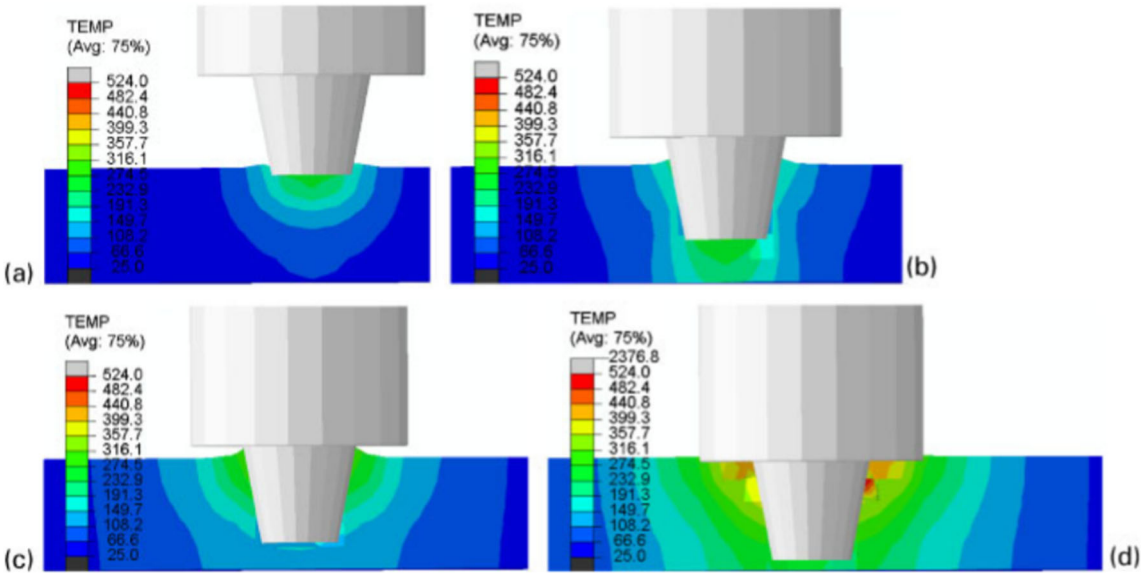

Fig. 14 Temperature profile at different locations of the plunge stage [102]

normal to the interface can be calculated in Eq. 3, where x is the thickness of the IMC, t is the welding time, and k is a growth constant. The constant k can be calculated by the Arrhenius relationship through Eq. 4, where k_0 is the pre-exponent factor, Q is the activation energy, R is the gas constant, and T is the temperature. Both the welding time and the temperature profiles were extracted from the developed thermal model. The calculated IMC layer thickness is half of the experimental measurement, which indicates that more improvements were needed.

$$\frac{dx}{dt} = kt^{-0.5} \tag{3}$$

$$k = k_0 e^{\frac{-Q}{RT}} \tag{4}$$

Heidarzadeh et al. [107] developed a thermal-mechanical model to predict the mechanical properties of FSW welds of pure copper with the commercial finite element code COMSOL. The grain size is calculated based on the following:

$$Q = 3\gamma\left(\frac{1}{G_i} - \frac{1}{G_f}\right) \tag{5}$$

where Q is the energy released by grain growth, G_i is the initial grain size, G_f is the final grain size, and γ is the areal energy density of grain boundary. The authors used the modified Eq. 5 to calculate the grain growth through the generated heat during the FSSW process. The calculated grain size fit well with the experimental results at different tool rotation speeds. The dominant factor in determining the grain size was shown to be the peak temperature during the welding process. Furthermore, the model can be applied to calculate the micro-hardness distribution of the stirring zone according to the Hall-Petch relationship, as shown in Eq. 6

$$HV = 66.433 + 80.6 \times d^{-0.5} \tag{6}$$

where HV is the micro-hardness and d is the average grain size. Finally, the authors applied Eq. 7 for the prediction of the UTS for the welding.

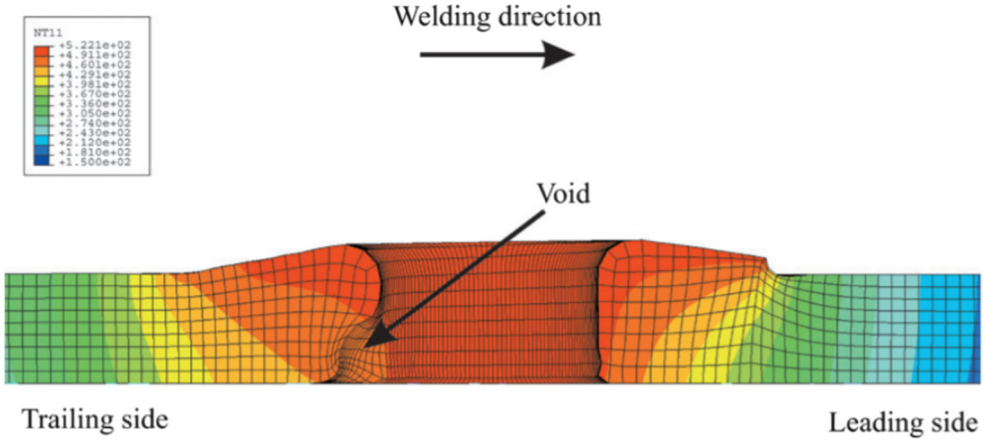

Fig. 15 Void formation during the friction stir welding process [104]

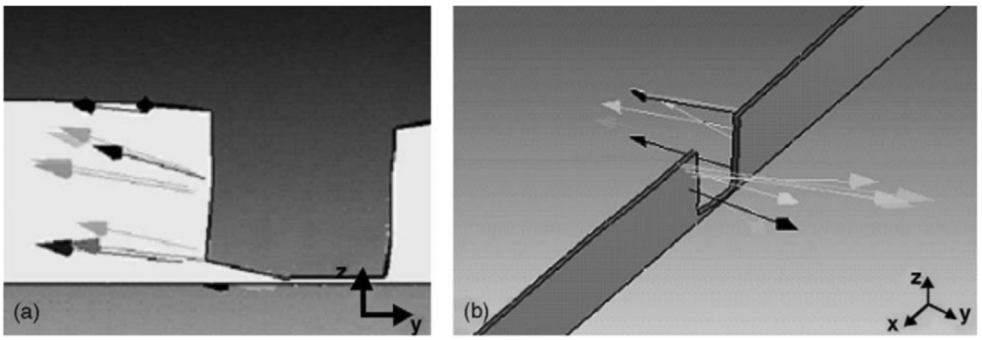

Fig. 16 Material flow in the welding zone [108]

$$UTS = 1.17 \times \left(12.77 + 520 \times d^{-0.5}\right) \quad (7)$$

where *UTS* is the ultimate tensile strength and d is the average grain size. The calculated UTS agreed well with the experimental results.

Buffa et al. [108] applied the FEA software DEFORM-3D to model the FSW process of Al7075. Their model was capable of predicting the material flow pattern during the welding process, which is shown by arrows in Fig. 16. It was observed that there was no vertical material flow around the cylindrical pin. In the meantime, the authors found that a different pin shape was likely to cause an additional downward flow of the material, which creates a helical movement.

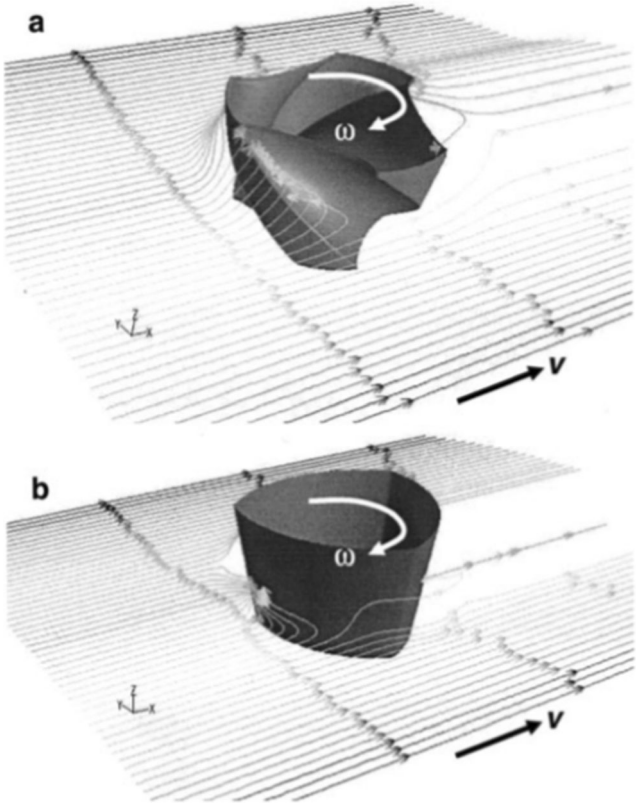

Fig. 17 Comparison of streamline for material flow between **a** Triffute and **b** Trivex tool [110]

3.2 Fluid dynamics approach

Fluid dynamics is another main approach to solve the coupled thermal-mechanical problem of the FSW process. In this method, the material is treated as a non-Newtonian fluid with high viscosities and the model is formulated in the Eulerian coordination system with fixed mesh. In this case, the excessive element distortion can be avoided and large material deformation can be efficiently captured by the model. Since for fluid, the only mechanical property is the viscosity. Based on available constitutive material model for plastic deformation, the equation generally adopted to calculate the equivalent viscosity is as the following:

$$\mu = \frac{\sigma_e}{3\dot{\varepsilon}_e} \quad (8)$$

Ulysse [109] developed a three-dimensional visco-plastic fluid model for friction stir welding of Al 7050 using the commercial software FIDAP. The rigid visco-plastic material properties were implemented into the model, where the material flow stress is a function of strain rate and temperature. The thermal conductivity and the specific heat coefficients were also temperature-dependent. A good agreement of the temperature history and force profile was achieved between the model results and the experimental data. Colegrove et al. [110] studied effects of different tool pin designs on the material flow behavior with the computational fluid dynamics (CFD) software FLUENT. The calculated material flow streamline plots showed a strong augering action of the Triflute tool, which caused a higher down-force. A greater vertical movement with the Triflute tool was observed, as shown in Fig. 17.

Hossfeld et al. [111] used the coupled Eulerian-Lagrangian (CEL) method in Abaqus to model FSW of Al 6061. The workpiece was treated as the Eulerian part while the tool was the Lagrangian part. The modeling results showed a localized high temperature region and a high temperature gradient along the welding direction. The model was also capable of predicting the void formation at the bottom behind the tool, as shown

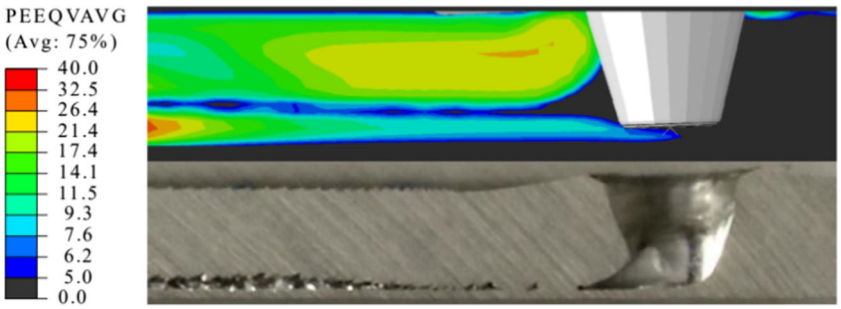

Fig. 18 Void formation at the bottom behind the tool [111]

in Fig. 18. Similarly, Li et al. [112] applied ABAQUS/CEL approach to determine material flow in FSW of Al2024. The relative difference between the calculated peak temperature and the experimental results was 6.34%.

Chu et al. [113] developed a numerical model for analyzing material flow during FSSW of Al2098 with ABAQUS. The numerically determined temperature profiles and material deformation distribution agreed well with the experimental data, as shown in Fig. 19.

Another group of fluid-based FSW model is the smooth particle hydrodynamics (SPH) approach [114–116]. SPH is a Lagrangian particle–based meshless method, where all the field variables, such as mass, momentum, and temperature, are associated with particles. It has a better capability in tracking free surface and interface. However, physically SPH is still treating FSW as a fluid flow problem.

3.3 Modeling on FSW of dissimilar materials

All the abovementioned models focus on FSW of joining same material. Limited amount of open literature discussed

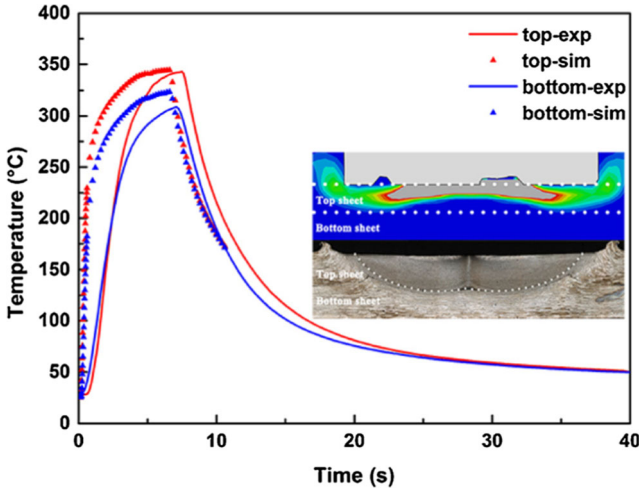

Fig. 19 Comparison of the temperature and material deformation profiles between numerical and experimental results [113]

modeling of FSW for dissimilar materials. One of the challenges is to consider the interactions of two materials in the weld. Padmanaban et al. [117] developed a computational fluid dynamics (CFD)–based numerical model in the commercialized software FLUENT to predict temperature profile and material flow during FSW of Al2024 with Al7075. The welding process is considered as a laminar flow past a steady rotating welding tool, which was shown in Fig. 20. The developed model was validated by the temperature profile at different welding speeds, and the model results are consistent with the experimental data. According to the developed model, as the tool rotation speed increased, the material viscosity decreased, which enhanced the material flow and created a larger stir zone around the tool pin.

Fadi et al. [118] developed a thermomechanical model for FSSW Al6061 and Al5083 with the software of Abaqus. Plastic behaviors of the two materials are both modeled with the Johnson-Cook law. Control volume approach was applied for analyzing the two materials in the workpiece region while the tool was modeled as a rigid Lagrangian body. Interaction between the tool and workpiece was described with Coulomb's friction model and the frictional coefficient was set at 0.8. The estimated peak temperature was higher than the experimental data. The possible reason behind it related to the precision in temperature measurements due to the poor

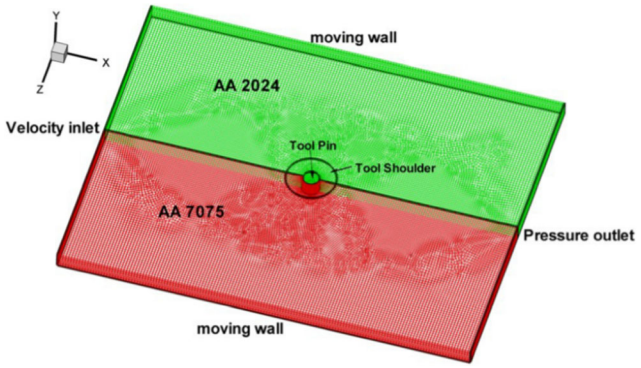

Fig. 20 Modeling setup for FSW of dissimilar materials [117]

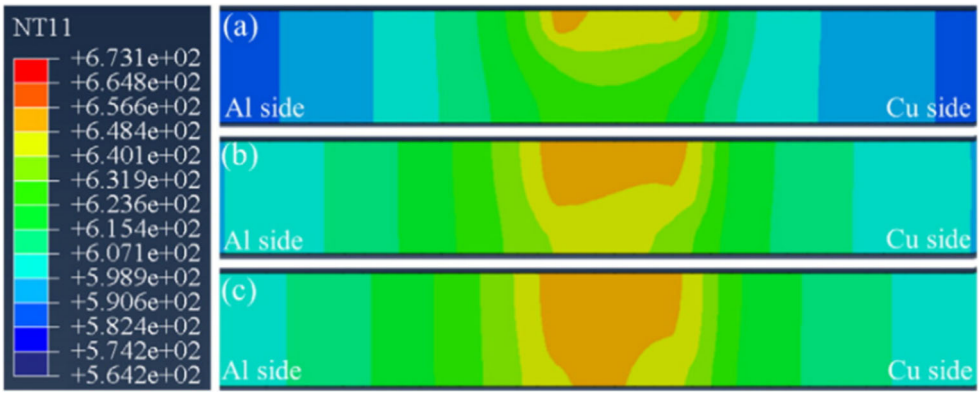

Fig. 21 Temperature distribution at different depths during the plunge stage [119]

thermocouple connectivity. Yaduwanshi et al. [119] developed a model for the plasma-assisted FSW of aluminum and copper in ABAQUS. To account for the behavior of two materials in the welding zone, the authors applied the concept of time varying functionally graded material (FGM) and mixture rule, which can incorporate the volume fraction, specific heat and mass density of different materials. The authors calculated the temperature evolution during the plunge stage. A higher thermal profile was observed in the aluminum side due to its higher thermal conductivity, as shown in Fig. 21.

Liu et al. [120] modeled the transient plunge stage during FSW of Al 6061 to TRIP 780 steel using the ABAQUS/Explicit program. A field variable is applied to identify the two materials in the weld zone, where the corresponding physical and mechanical properties are assigned during numerical calculation. Their estimated axial force correlated well with the experimental results at the beginning of the plunge stage. Higher temperature distribution and stress field are shown on the steel side compared with aluminum. For the steady-state welding stage during FSW of Al 6061 to TRIP 780 steel, Liu et al. [121] developed a CFD model in the FLUENT software, where volume of fluid (VOF) method is adopted. The two materials are considered as multiple phases in the stirring nugget. In this method, the velocity, temperature, and pressure fields are shared among the two materials while the physical properties are averaged based on the volume fraction of each material in the specific element. A shear stress tool-workpiece frictional boundary condition is applied,

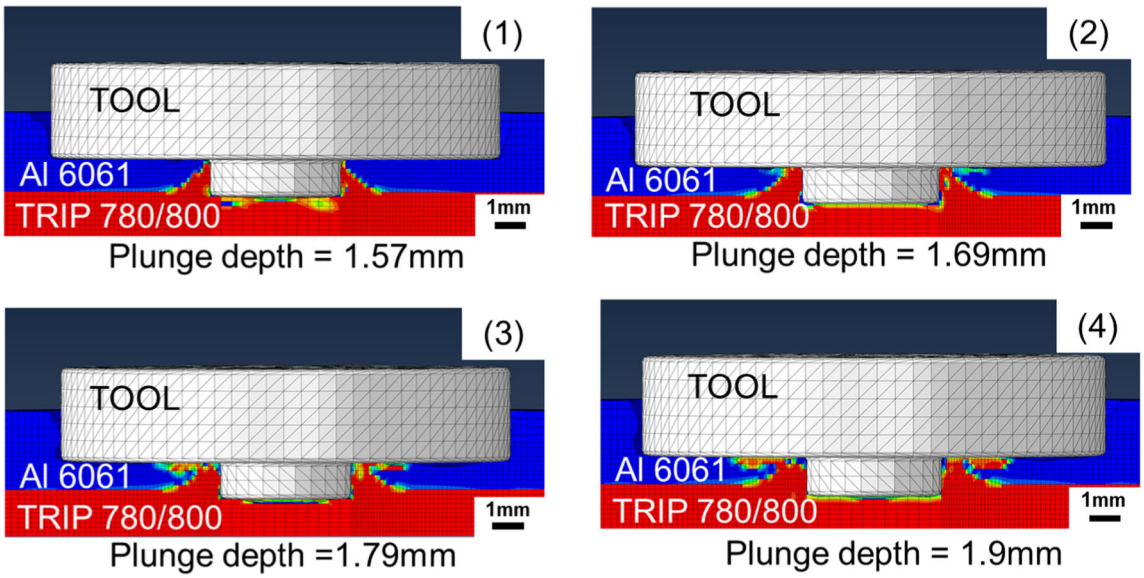

Fig. 22 Material distribution at different plunge depths during FSSW of Al 6061 to TRIP steel [122]

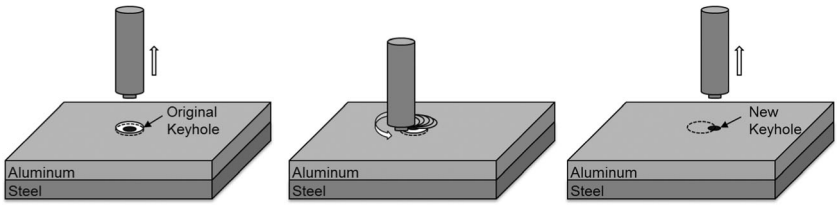

Fig. 23 Schematic illustration of keyhole refilled FSSW process [129]

which greatly improved the material distribution calculation results compared with empirical velocity based boundary condition. Chen et al. [122] modeled FSSW of Al 6061 to TRIP 780 steel using the ABAQUS/CEL algorithm. The penalty method was utilized to determine the interaction force between the Lagrangian tool and Eulerian workpiece. Mixture theories are applied to consider the two materials involved in the stirring zone. The authors showed the material distribution at different plunge depths and the model is also capable to predict formation of the hook, as shown in Fig. 22.

Li et al. [123] applied the functionally graded material (FGM) and introduced the parameter of distribution coefficient to model the material field in the weld nugget. The rule of mixture was then adopted for averaging material properties. Simulation of the steady-state welding process was conducted in ABAQUS with user-defined subroutine DFLUX for modeling the moving heat source. The model was validated with the calculated residual stress. Torres et al. [124] developed a computational fluid dynamics model based on COMSOL for simulating the temperature distribution and thermal history during stable welding stage of Al 6061 and AISI SAE 1020 steel. Their heat generation model was based on studies from Nandan and Debroy [25, 125–128]. However, no material distribution was provided.

4 Innovative variants of friction stir–related process

In recent years, many innovative variants have been developed to improve traditional friction stir–related processes. Chen et al. [129] developed a new keyhole refilled FSSW process to weld the aluminum alloy with the TRIP 780/800 steel, which consisted of two steps. In the first step, conventional FSSW was performed, where a rotating cylinder tool plunged into the base materials at the desired depth, dwelled a certain amount of time, and then retracted from the workpiece. In the second step, the welding tool was shifted a certain distance away from the location of the original keyhole center. The tool then re-plunged into the base materials with a smaller depth and traveled along a circular path surrounding the keyhole with a pre-assigned radius and traveling speed. In this way, the original keyhole was refilled and the final tool retraction leaves a much smaller keyhole on the weld. The process described above is schematically shown in Fig. 23. The keyhole is effectively refilled with this method. The joint strength and elongation are enhanced by 56.33% and 81.25% respectively compared with the conventional FSSW. Besides, reliability of the welding process was greatly improved.

Liu et al. [130] performed electrically assisted friction stir welding of aluminum to steel. Their experimental setup is shown in Fig. 24. The two electrodes were placed on the top

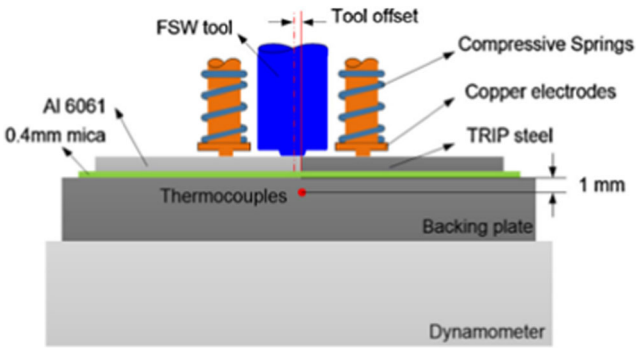

Fig. 24 Schematic illustration of electrically assisted FSW by Liu et al. [130]

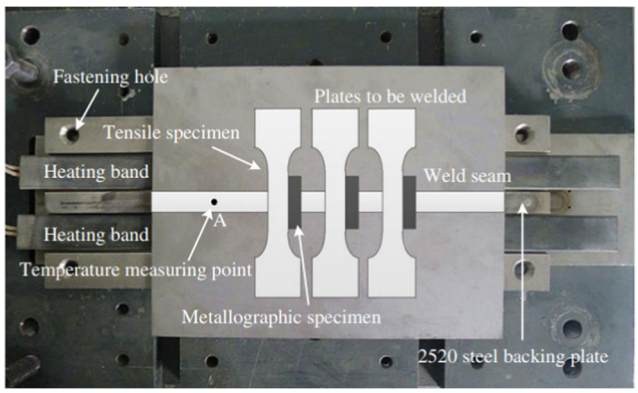

Fig. 25 Experimental setup for the back heating assisted FSW [132]

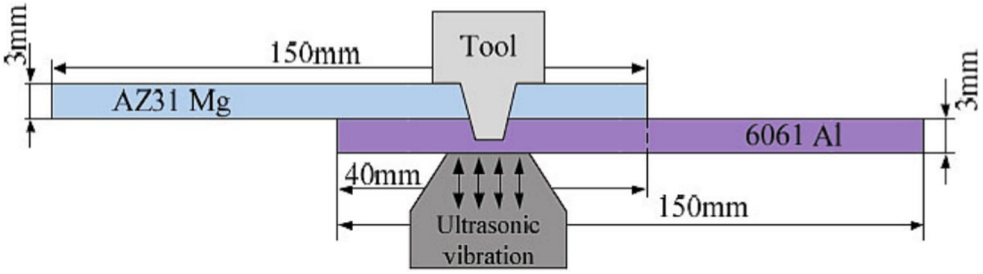

Fig. 26 Illustration of the ultrasonic assisted FSW process [134]

surface of the workpiece materials and traveled together with the FSW tool during the welding process. In this configuration, the electrical current flowed through the weld center of the two base materials and the FSW tool was only passively involved in the circuit. The welding force is shown to be effectively reduced under the assistance of electrical current. They attributed this as a synergic effect of direct material softening through electro-plasticity [131] and thermal softening through Joule heating.

Ji et al. [132] studied the effect of temperature of backing plate on friction stir welding of Ti-6Al-4V. In their experiments, the heating band was placed under the workpiece, as shown in Fig. 25. The authors mentioned that when the rotation speed is in the range of 120 to 200 rpm, void defects could be generated in the stir zone. With the supplementary heating source under the workpiece, the temperature profile along the thickness direction is more uniform, which can promote plasticized material flow and eliminate potential void defects in the stirring zone. Moreover, the tool wear was ameliorated.

The benefits of ultrasonic vibration has also investigated in the hybrid friction stir welding process, since it can soften the material through acoustic-plastic effect [133] and also modify the frictional behavior. Ji et al. [134] applied a perpendicular ultrasonic vibration at the backing anvil during FSSW of AZ31 Mg alloy to 6061 Al alloy, as shown in Fig. 26. Upward flow of the lower sheet material is enhanced and a better mixing between dissimilar materials is achieved. Ultrasonic vibration also showed to refine the grain size. IMCs were found at the interface between the steel and aluminum, which mainly consist of Al_3Mg_2 and $Al_{12}Mg_{17}$. Thoma et al. [135] applied a lateral ultrasonic vibration during FSW of aluminum to steel, as shown in Fig. 27. Less amount and smaller sizes of the Al-Fe intermetallic particles are observed in the stirring zone under the ultrasonically assisted condition. Liu et al. [136] applied an ultrasonic pretreatment on the workpiece in front of the FSW tool, as shown in Fig. 28. The ultrasonic vibration is reported to enlarge the volume of deformed material surrounding the pin and can increase the welding speed without generation of wormhole defects.

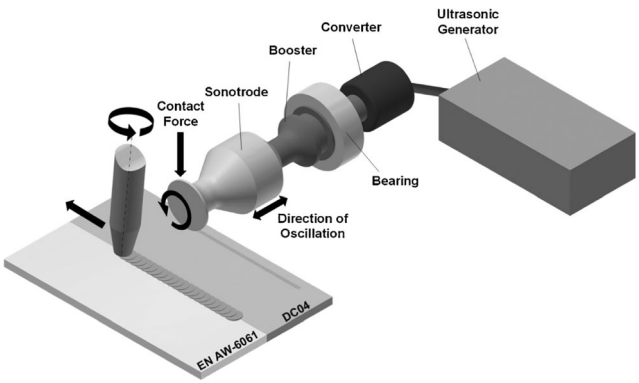

Fig. 27 Illustration of lateral ultrasonic vibration assisted FSW process [135]

Gupta et al. [137] applied the friction stir scribe welding for joining the Al6022 and low carbon electro-galvanized steel sheets. This welding tool design was first used by Jana et al. [138]. A 1-mm-diameter tungsten carbide scribe protruded from the bottom tip of the pin, as shown in Fig. 29 and the pin is made of H13 tool steel. This specially designed tool pin scribes the upper surface of the steel and upsets a small amount of material, which creates a mechanical interlocking between the steel and aluminum. The highest joint strength during lap shear tensile tests reached 5.8 kN. There were no significant differences of the joint strength between retreating and advancing sides of the weld.

Mofid et al. [139] performed submerged friction stir welding under water to improve the joint property between Al alloy 5083 and AZ31C-O Mg alloy. The thickness of both sheets is 3 mm. They reported that conventional FSW produced Al_3Mg_2, $Al_{12}Mg_{17}$, and Al_2Mg_3 intermetallic phases at the welding interface. As a comparison, for underwater FSW, the peak temperature decreased 25 °C (Fig. 30). The joint showed a much smoother interface and less intermixing of the base materials. Furthermore, less amount of intermetallic compounds is formed.

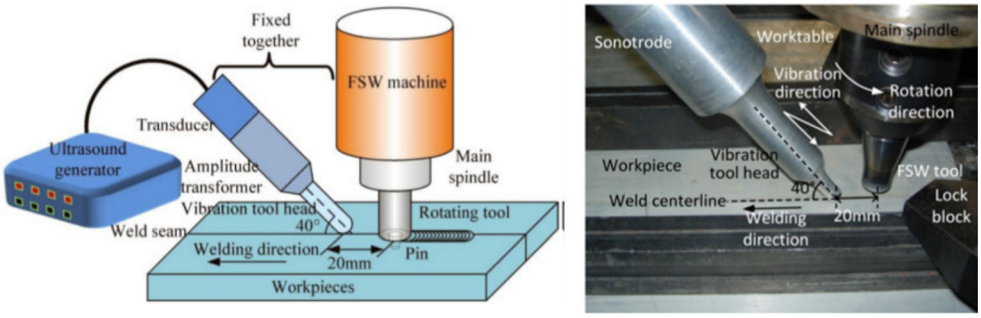

Fig. 28 Illustration of ultrasonic pre-treatment on the workpiece [136]

Evans et al. [140] developed a friction stir extraction (FSE) process for joining aluminum to steel. Groove features were pre-machined onto the steel surface. During the welding process, the aluminum sheet on the top was squeezed into the groove due to the large plunge force of the welding tool. Two types of groove features were investigated, including two slit saw groove and O-ring groove, as shown in Fig. 31. The macroscopic mechanical interlocking between the steel and aluminum greatly increased the joint strength. In the meantime, the welding tool did not touch the steel on the bottom, which is highly beneficial for tool life.

Similarly, Reza-E-Rabby et al. [141] applied friction stir dovetailing (FSD) process to join the thick section Al6061 (38.1 mm) to steel plate (12.7 mm). The steel is pre-machined with groove features and inserted into the Al6061, which forms a sandwich structure, as shown in Fig. 32. FSD showed to be capable of making strong joints between steel and aluminum. Formation of IMCs helps to improve the joint strength. Different groove geometries had been investigated for the optimal configuration. The nested grooves showed to provide the highest strength based on multiple mechanical interlocking that resisted deformation in the tensile direction.

Fig. 29 Friction stir scribe pin tool [137]

5 Summary and future work

Friction stir–related welding processes are advantageous in joining dissimilar materials based on its solid-state nature and avoidance of bulk material melting. The amount of brittle IMCs can be controlled to be lower than the critical value for a desirable joint strength. This paper reviewed the experimental works of several processes for joining dissimilar materials, including friction stir welding, friction stir lap welding, friction stir spot welding, and keyhole refilled friction stir welding process. Then, the associated modeling works are summarized, including process models to evaluate the material flow and temperature evolution as well as microstructure and property model to determine the weld quality. This provides fundamentals in the field of integrated computational material engineering (ICME) for friction stir welding. Finally, several recent innovative variants of friction stir–related process are discussed, which are developed to further improve the process and enhance dissimilar material joint quality.

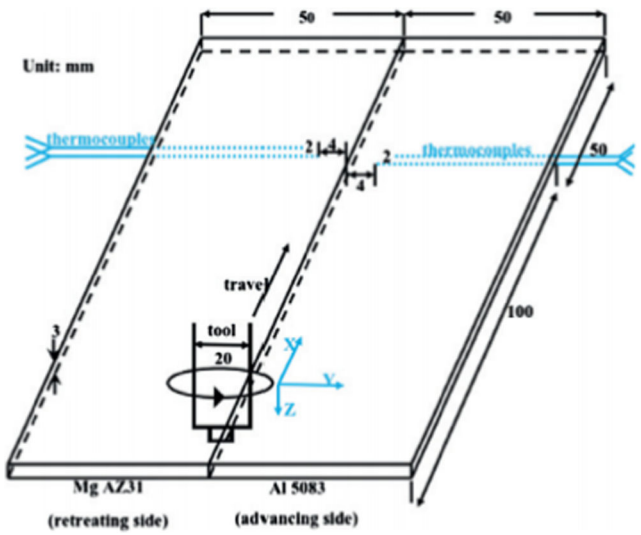

Fig. 30 Illustration of the underwater friction stir welding [139]

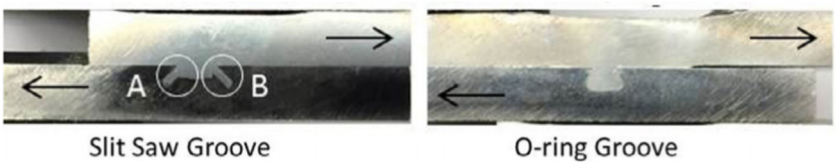

Fig. 31 Weld made with slit saw groove and O-ring groove [140]

Some possible future research works in the field of friction stir–related processes are proposed as following:

- Development of integrated friction stir models that based on input tool geometry and process parameters can determine the formation of potential weld defects and joint strength: In the process level, more accurate material constitutive model and friction model need to be developed, which helps to better capture the coupled thermomechanical behavior of the friction stir process. In the microstructure level, effects of severe plastic deformation on the thermomechanical and kinetic rules need to be considered. Particularly for dissimilar material joining, calculating the formation and growth of IMCs is critical in predicting the final joint quality.
- Solution of the corrosion issues of dissimilar material welds: Even though friction stir–related process is capable to produce sound joints between different materials, degenerated corrosion property of the joints has been a concern. Effective solution of the corrosion issue can substantially expand dissimilar material welds in structural applications.
- Improvement in the keyhole refilling process: Existing techniques for refilling keyhole relies on a specially designed machine and tool system. The process can be challenging when advanced high-strength steel is involved as one of the workpiece materials.
- Development of faster friction stir–related process: Even though the solid-state nature provides these processes with several intrinsic advantages, the processing speed is generally unsatisfactory compared with corresponding fusion welding techniques. For example, currently, the productivity of friction stir welding can hardly match conventional arc welding or laser welding process. Moreover, friction stir spot welding is much slower compared with resistance spot welding.
- Improvement of energy efficiency in hybrid friction stir welding process: Even though external energies, such as electrical current and ultrasonic vibration shows promising results in improving conventional friction stir–related process, including higher welding speed, reduced welding force, and increased joint strength. However, the total energy efficiency can be low for the hybrid process compared with traditional friction stir–related process. Better design of the hybrid process needs to be developed to maximize the benefits of external energy.

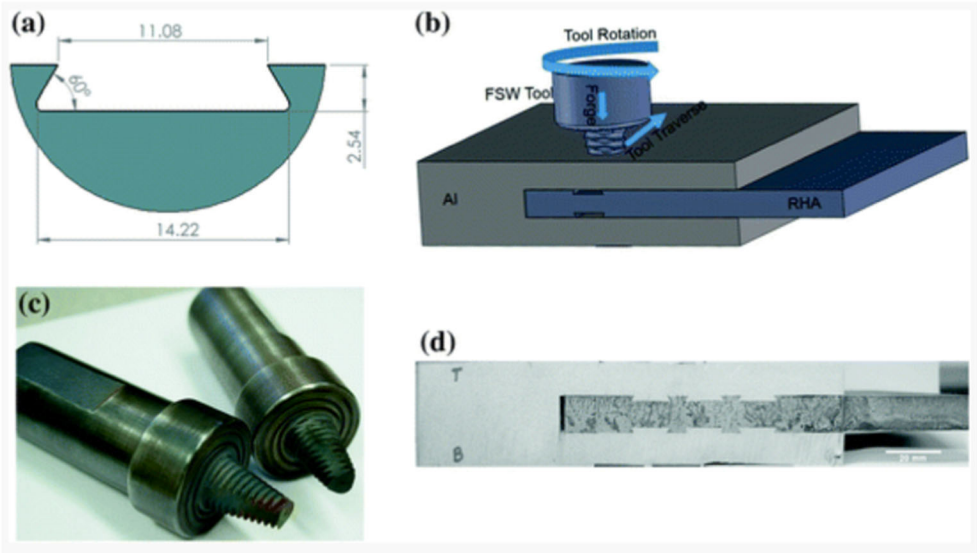

Fig. 32 Illustration of the FSD of dissimilar materials [141]

References

1. Han L, Thornton M, Li D, Shergold M (2011) Effect of governing metal thickness and stack orientation on weld quality and mechanical behaviour of resistance spot welding of AA5754 aluminium. Mater Des 32(4):2107–2114
2. Nanda T, Singh V, Singh V, Chakraborty A, Sharma S (2019) Third generation of advanced high-strength steels: Processing routes and properties. Proceedings of the Institution of Mechanical Engineers, Part L: Journal of Materials: Design and Applications 233(2):209–238
3. Sun X, Stephens EV, Khaleel MA (2008) Effects of fusion zone size and failure mode on peak load and energy absorption of advanced high strength steel spot welds under lap shear loading conditions. Eng Fail Anal 15(4):356–367
4. Kuziak R, Kawalla R, Waengler S (2008) Advanced high strength steels for automotive industry. Arch Civil Mech Eng 8(2):103–117
5. Kwon O, Lee KY, Kim GS, Chin KG (2010) New Trends in Advanced High Strength Steel Developments for Automotive Application. Materials Science Forum 638–642:136–141
6. Matlock DK, Speer JG, Moor ED, Gibbs PJ (2012) Recent developments in advanced high strength sheet steels for automotive applications: an overview. JESTECH 15(1):1–12
7. Long X, Khanna SK (2007) Fatigue properties and failure characterization of spot welded high strength steel sheet. Int J Fatigue 29(5):879–886
8. Badarinarayan H, Yang Q, Zhu S (2009) Effect of tool geometry on static strength of friction stir spot-welded aluminum alloy. Int J Mach Tools Manuf 49(2):142–148
9. Qiu R, Iwamoto C, Satonaka S (2009) The influence of reaction layer on the strength of aluminum/steel joint welded by resistance spot welding. Mater Charact 60(2):156–159
10. Qiu R, Iwamoto C, Satonaka S (2009) Interfacial microstructure and strength of steel/aluminum alloy joints welded by resistance spot welding with cover plate. J Mater Process Technol 209(8): 4186–4193
11. Sun X, Stephens EV, Khaleel MA, Shao H, Kimchi M (2004) Resistance spot welding of aluminum alloy to steel with transition material-from process to performance-part I: experimental study. Weld J 83:188-S
12. Qiu R, Satonaka S, Iwamoto C (2009) Effect of interfacial reaction layer continuity on the tensile strength of resistance spot welded joints between aluminum alloy and steels. Mater Des 30(9):3686–3689
13. Ambroziak A, Korzeniowski M (2010) Using resistance spot welding for joining aluminium elements in automotive industry. Arch Civil Mech Eng 10(1):5–13
14. Hao M, Osman K, Boomer D, Newton C (1996) Developments in characterization of resistance spot welding of aluminum. Weld J 75(1):1–4 Including Welding Research Supplement
15. Florea R, Bammann D, Yeldell A, Solanki K, Hammi Y (2013) Welding parameters influence on fatigue life and microstructure in resistance spot welding of 6061-T6 aluminum alloy. Mater Des 45:456–465
16. Lindenburg R, Braton N (1976) Aluminum welding, welding and other joining processes. Allyn and Bacon, Inc., Boston
17. Han L, Thornton M, Boomer D, Shergold M (2010) Effect of aluminium sheet surface conditions on feasibility and quality of resistance spot welding. J Mater Process Technol 210(8):1076–1082
18. Fukumoto S, Lum I, Biro E, Boomer D, Zhou Y (2003) Effects of electrode degradation on electrode life in resistance spot welding of aluminum alloy 5182. Weld J 82(11):307-S
19. Florea R, Solanki K, Bammann D, Baird J, Jordon J, Castanier M (2012) Resistance spot welding of 6061-T6 aluminum: failure loads and deformation. Mater Des 34:624–630
20. Mishra RS, Ma Z (2005) Friction stir welding and processing. Mater Sci Eng R Rep 50(1):1–78
21. Thomas W, Nicholas E, Needham J, Murch M, Temple-Smith P, Dawes C (1991) Friction stir butt welding, International Patent Appl. n. PCT/GB92/02203 and GB Patent Appl. n. 9125978.8," US Patent(5,460,317)
22. Rao H, Yuan W, Badarinarayan H (2015) Effect of process parameters on mechanical properties of friction stir spot welded magnesium to aluminum alloys. Mater Des (1980–2015) 66:235–245
23. Chen K, Liu X, Ni J. Effects of process parameters on friction stir spot welding of aluminum alloy to advanced high-strength steel, Proc. ASME 2016 11th International Manufacturing Science and Engineering Conference, American Society of Mechanical Engineers, pp V001T002A011–V001T002A011
24. Bilici MK, Yükler Aİ, Kurtulmuş M (2011) The optimization of welding parameters for friction stir spot welding of high density polyethylene sheets. Mater Des 32(7):4074–4079
25. Nandan R, DebRoy T, Bhadeshia H (2008) Recent advances in friction-stir welding–process, weldment structure and properties. Prog Mater Sci 53(6):980–1023
26. Seidel T, Reynolds AP (2001) Visualization of the material flow in AA2195 friction-stir welds using a marker insert technique. Metall Mater Trans A 32(11):2879–2884
27. Balasubramanian V (2008) Relationship between base metal properties and friction stir welding process parameters. Mater Sci Eng A 480(1–2):397–403
28. Iwashita T (2003) Method and apparatus for joining, Google Patents
29. Feng Z, Santella M, David S, Steel R, Packer S, Pan T, Kuo M, Bhatnagar R (2005) Friction stir spot welding of advanced high-strength steels-a feasibility study, No. 0148-7191, SAE Technical Paper
30. Zhang Z, Yang X, Zhang J, Zhou G, Xu X, Zou B (2011) Effect of welding parameters on microstructure and mechanical properties of friction stir spot welded 5052 aluminum alloy. Mater Des 32(8–9):4461–4470
31. Freeney T, Sharma S, Mishra R (2006) Effect of welding parameters on properties of 5052 Al friction stir spot welds, No. 0148-7191, SAE Technical Paper
32. Badarinarayan H, Shi Y, Li X, Okamoto K (2009) Effect of tool geometry on hook formation and static strength of friction stir spot welded aluminum 5754-O sheets. Int J Mach Tools Manuf 49(11): 814–823
33. Pathak N, Bandyopadhyay K, Sarangi M, Panda SK (2013) Microstructure and mechanical performance of friction stir spot-welded aluminum-5754 sheets. J Mater Eng Perform 22(1):131–144
34. Tozaki Y, Uematsu Y, Tokaji K (2007) Effect of tool geometry on microstructure and static strength in friction stir spot welded aluminium alloys. Int J Mach Tools Manuf 47(15):2230–2236
35. Wang D-A, Lee S-C (2007) Microstructures and failure mechanisms of friction stir spot welds of aluminum 6061-T6 sheets. J Mater Process Technol 186(1):291–297
36. Wang D-A, Chen C-H (2009) Fatigue lives of friction stir spot welds in aluminum 6061-T6 sheets. J Mater Process Technol 209(1):367–375
37. Awang M, Mucino VH (2010) Energy generation during friction stir spot welding (FSSW) of Al 6061-T6 plates. Mater Manuf Process 25(1–3):167–174
38. Rodrigues D, Loureiro A, Leitao C, Leal R, Chaparro B, Vilaça P (2009) Influence of friction stir welding parameters on the microstructural and mechanical properties of AA 6016-T4 thin welds. Mater Des 30(6):1913–1921

39. Shen Z, Yang X, Yang S, Zhang Z, Yin Y (2014) Microstructure and mechanical properties of friction spot welded 6061-T4 aluminum alloy. Mater Des (1980–2015) 54:766–778
40. Mitlin D, Radmilovic V, Pan T, Chen J, Feng Z, Santella M (2006) Structure–properties relations in spot friction welded (also known as friction stir spot welded) 6111 aluminum. Mater Sci Eng A 441(1):79–96
41. Su J-Q, Nelson T, Mishra R, Mahoney M (2003) Microstructural investigation of friction stir welded 7050-T651 aluminium. Acta Mater 51(3):713–729
42. Shen Z, Yang X, Zhang Z, Cui L, Li T (2013) Microstructure and failure mechanisms of refill friction stir spot welded 7075-T6 aluminum alloy joints. Mater Des 44:476–486
43. Bozzi S, Helbert-Etter A, Baudin T, Criqui B, Kerbiguet J (2010) Intermetallic compounds in Al 6016/IF-steel friction stir spot welds. Mater Sci Eng A 527(16):4505–4509
44. Liyanage T, Kilbourne J, Gerlich AP, North TH (2009) Joint formation in dissimilar Al alloy/steel and Mg alloy/steel friction stir spot welds. Sci Technol Weld Join 14(6):500–508
45. Taban E, Gould JE, Lippold JC (2010) Dissimilar friction welding of 6061-T6 aluminum and AISI 1018 steel: properties and microstructural characterization. Mater Des 31(5):2305–2311
46. Chen YC, Gholinia A, Prangnell PB (2012) Interface structure and bonding in abrasion circle friction stir spot welding: a novel approach for rapid welding aluminium alloy to steel automotive sheet. Mater Chem Phys 134(1):459–463
47. Da Silva A, Aldanondo E, Alvarez P, Arruti E, Echeverria A (2010) Friction stir spot welding of AA 1050 Al alloy and hot stamped boron steel (22MnB5). Sci Technol Weld Join 15(8): 682–687
48. Fereiduni E, Movahedi M, Kokabi A (2015) Aluminum/steel joints made by an alternative friction stir spot welding process. J Mater Process Technol 224:1–10
49. Shi Y, Yue Y, Zhang L, Ji S, Wang Y (2018) Refill friction stir spot welding of 2198-T8 aluminum alloy. Trans Indian Inst Metals 71(1):139–145
50. Schilling C, dos Santos J (2004) Method and device for joining at least two adjoining work pieces by friction welding, Google Patents
51. Zhao YQ, Liu HJ, Chen SX, Lin Z, Hou JC (2014) Effects of sleeve plunge depth on microstructures and mechanical properties of friction spot welded alclad 7B04-T74 aluminum alloy. Mater Des (1980–2015) 62:40–46
52. Reimann M, Goebel J, dos Santos JF (2017) Microstructure and mechanical properties of keyhole repair welds in AA 7075-T651 using refill friction stir spot welding. Mater Des 132:283–294
53. Chen Y, Chen J, Shalchi Amirkhiz B, Worswick MJ, Gerlich AP (2015) Microstructures and properties of Mg alloy/DP600 steel dissimilar refill friction stir spot welds. Sci Technol Weld Join 20(6):494–501
54. Shen Z, Ding Y, Chen J, Gerlich A (2016) Comparison of fatigue behavior in Mg/Mg similar and Mg/steel dissimilar refill friction stir spot welds. Int J Fatigue 92:78–86
55. Shen Z, Chen J, Ding Y, Hou J, Shalchi Amirkhiz B, Chan K, Gerlich A (2017) Role of interfacial reaction on the mechanical performance of Al/steel dissimilar refill friction stir spot welds. Sci Technol Weld Join:1–16
56. Sahu PK, Pal S, Pal SK, Jain R (2016) Influence of plate position, tool offset and tool rotational speed on mechanical properties and microstructures of dissimilar Al/Cu friction stir welding joints. J Mater Process Technol 235:55–67
57. Liu X, Lan S, Ni J (2014) Analysis of process parameters effects on friction stir welding of dissimilar aluminum alloy to advanced high strength steel. Mater Des 59:50–62
58. Habibnia M, Shakeri M, Nourouzi S, Givi MB (2015) Microstructural and mechanical properties of friction stir welded 5050 Al alloy and 304 stainless steel plates. Int J Adv Manuf Technol 76(5–8):819–829
59. Xue P, Ni D, Wang D, Xiao B, Ma Z (2011) Effect of friction stir welding parameters on the microstructure and mechanical properties of the dissimilar Al–Cu joints. Mater Sci Eng A 528(13–14): 4683–4689
60. Fu B, Qin G, Li F, Meng X, Zhang J, Wu C (2015) Friction stir welding process of dissimilar metals of 6061-T6 aluminum alloy to AZ31B magnesium alloy. J Mater Process Technol 218:38–47
61. Yue Y, Li Z, Ji S, Huang Y, Zhou Z (2016) Effect of reverse-threaded pin on mechanical properties of friction stir lap welded alclad 2024 aluminum alloy. J Mater Sci Technol 32(7):671–675
62. Ge Z, Gao S, Ji S, Yan D (2018) Effect of pin length and welding speed on lap joint quality of friction stir welded dissimilar aluminum alloys. Int J Adv Manuf Technol 98(1–9):1461–1469
63. Balakrishnan M, Leitão C, Arruti E, Aldanondo E, Rodrigues D (2018) Influence of pin imperfections on the tensile and fatigue behaviour of AA 7075-T6 friction stir lap welds. Int J Adv Manuf Technol:1–11
64. Saeid T, Abdollah-Zadeh A, Sazgari B (2010) Weldability and mechanical properties of dissimilar aluminum–copper lap joints made by friction stir welding. J Alloys Compd 490(1–2):652–655
65. Chen Y, Nakata K (2009) Effect of tool geometry on microstructure and mechanical properties of friction stir lap welded magnesium alloy and steel. Mater Des 30(9):3913–3919
66. Lee C-Y, Choi D-H, Yeon Y-M, Jung S-B (2009) Dissimilar friction stir spot welding of low carbon steel and Al–Mg alloy by formation of IMCs. Sci Technol Weld Join 14(3):216–220
67. Chowdhury S, Chen D, Bhole S, Cao X, Wanjara P (2012) Lap shear strength and fatigue life of friction stir spot welded AZ31 magnesium and 5754 aluminum alloys. Mater Sci Eng A 556: 500–509
68. Sato Y, Shiota A, Kokawa H, Okamoto K, Yang Q, Kim C (2010) Effect of interfacial microstructure on lap shear strength of friction stir spot weld of aluminium alloy to magnesium alloy. Sci Technol Weld Join 15(4):319–324
69. Prasomthong S, Sangsiri P, Kimapong K (2015) Friction stir spot welding of AA5052 aluminum alloy and C11000 copper lap joint. Int J Adv Cult Technol 3(1):145–152
70. Triwanapong S, Kaewwichit J, Roybang W, Kimapong K (2015) Optimization of friction stir spot welding parameters of lap joint between AA1100 aluminum alloy and SGACD zinc-coated steel. Int J Adv Cult Technol 3(1):161–168
71. Sun YF, Fujii H, Takaki N, Okitsu Y (2013) Microstructure and mechanical properties of dissimilar Al alloy/steel joints prepared by a flat spot friction stir welding technique. Mater Des 47:350–357
72. Figner MSG, Vallant R, Weinberger MST, Enzinger N, Schröttner H, Pašič H (2009) Friction stir spot welds between aluminium and steel automotive sheets: influence of welding parameters on mechanical properties and microstructure. Weld World 53(1–2):R13–R23
73. Hong SH, Sung S-J, Pan J (2015) Failure mode and fatigue behavior of dissimilar friction stir spot welds in lap-shear specimens of transformation-induced plasticity steel and hot-stamped boron steel sheets. J Manuf Sci Eng 137(5):051023
74. Piccini JM, Svoboda HG (2015) Effect of pin length on friction stir spot welding (FSSW) of dissimilar aluminum-steel joints. Procedia Mater Sci 9:504–513
75. Lin Y-C, Chen J-N (2015) Influence of process parameters on friction stir spot welded aluminum joints by various threaded tools. J Mater Process Technol 225:347–356
76. Shen Z, Ding Y, Gopkalo O, Diak B, Gerlich A (2018) Effects of tool design on the microstructure and mechanical properties of refill friction stir spot welding of dissimilar Al alloys. J Mater Process Technol 252:751–759

77. Suhuddin U, Fischer V, Kroeff F, Dos Santos J (2014) Microstructure and mechanical properties of friction spot welds of dissimilar AA5754 Al and AZ31 Mg alloys. Mater Sci Eng A 590:384–389
78. Dong H, Chen S, Song Y, Guo X, Zhang X, Sun Z (2016) Refilled friction stir spot welding of aluminum alloy to galvanized steel sheets. Mater Des 94:457–466
79. Suhuddin U, Fischer V, Kostka A, dos Santos J (2017) Microstructure evolution in refill friction stir spot weld of a dissimilar Al–Mg alloy to Zn-coated steel. Sci Technol Weld Join 22(8):658–665
80. Ding Y, Shen Z, Gerlich A (2017) Refill friction stir spot welding of dissimilar aluminum alloy and AlSi coated steel. J Manuf Process 30:353–360
81. Fukada S, Ohashi R, Fujimoto M, Okada H Refill friction stir spot welding of dissimilar materials consisting of A6061 and hot dip zinc-coated steel sheets, Proc. Proceedings of the 1st international joint symposium on joining and welding. Elsevier, Amsterdam, pp 183–187
82. Reimann M, Gartner T, Suhuddin U, Göbel J, dos Santos JF (2016) Keyhole closure using friction spot welding in aluminum alloy 6061–T6. J Mater Process Technol 237:12–18
83. Cao JY, Wang M, Kong L, Guo LJ (2016) Hook formation and mechanical properties of friction spot welding in alloy 6061-T6. J Mater Process Technol 230:254–262
84. Rosendo T, Parra B, Tier M, Da Silva A, Dos Santos J, Strohaecker T, Alcântara N (2011) Mechanical and microstructural investigation of friction spot welded AA6181-T4 aluminium alloy. Mater Des 32(3):1094–1100
85. Oliveira P, Amancio-Filho S, Dos Santos J, Hage E (2010) Preliminary study on the feasibility of friction spot welding in PMMA. Mater Lett 64(19):2098–2101
86. Tier M, Rosendo T, dos Santos J, Huber N, Mazzaferro J, Mazzaferro C, Strohaecker T (2013) The influence of refill FSSW parameters on the microstructure and shear strength of 5042 aluminium welds. J Mater Process Technol 213(6):997–1005
87. Campanelli LC, Suhuddin UFH, Antonialli AÍS, dos Santos JF, de Alcantara NG, Bolfarini C (2013) Metallurgy and mechanical performance of AZ31 magnesium alloy friction spot welds. J Mater Process Technol 213(4):515–521
88. Li Z, Ji S, Ma Y, Chai P, Yue Y, Gao S (2016) Fracture mechanism of refill friction stir spot-welded 2024-T4 aluminum alloy. Int J Adv Manuf Technol 86(5–8):1925–1932
89. Khandkar M, Khan JA, Reynolds AP (2003) Prediction of temperature distribution and thermal history during friction stir welding: input torque based model. Sci Technol Weld Join 8(3): 165–174
90. Chao YJ, Qi X (1998) Thermal and thermo-mechanical modeling of friction stir welding of aluminum alloy 6061-T6. J Mater Process Manuf Sci 7:215–233
91. Chao YJ, Qi X, Tang W (2003) Heat transfer in friction stir welding—experimental and numerical studies. J Manuf Sci Eng 125(1):138–145
92. Zhu X, Chao Y (2004) Numerical simulation of transient temperature and residual stresses in friction stir welding of 304L stainless steel. J Mater Process Technol 146(2):263–272
93. Hamilton C, Dymek S, Blicharski M (2008) A model of material flow during friction stir welding. Mater Charact 59(9):1206–1214
94. De Vuyst T, D'Alvise L, Simar A, De Meester B, Pierret S (2005) Finite element modelling of friction stir welding of aluminium alloy plates-inverse analysis using a genetic algorithm. Weld World 49(3–4):47–55
95. Simar A, Lecomte-Beckers J, Pardoen T, De Meester B (2006) Effect of boundary conditions and heat source distribution on temperature distribution in friction stir welding. Sci Technol Weld Join 11(2):170–177
96. Song M, Kovacevic R (2003) Thermal modeling of friction stir welding in a moving coordinate system and its validation. Int J Mach Tools Manuf 43(6):605–615
97. Zhang H, Zhang Z, Chen J (2005) The finite element simulation of the friction stir welding process. Mater Sci Eng A 403(1):340–348
98. Kuykendall K, Nelson T, Sorensen C (2013) On the selection of constitutive laws used in modeling friction stir welding. Int J Mach Tools Manuf 74:74–85
99. Assidi M, Fourment L, Guerdoux S, Nelson T (2010) Friction model for friction stir welding process simulation: calibrations from welding experiments. Int J Mach Tools Manuf 50(2):143–155
100. Liechty B, Webb B (2008) Modeling the frictional boundary condition in friction stir welding. Int J Mach Tools Manuf 48(12–13): 1474–1485
101. Trimble D, Monaghan J, O'donnell G (2012) Force generation during friction stir welding of AA2024-T3. CIRP Ann Manuf Technol 61(1):9–12
102. Yu M, Li W, Li J, Chao Y (2012) Modelling of entire friction stir welding process by explicit finite element method. Mater Sci Technol 28(7):812–817
103. Mandal S, Rice J, Elmustafa AA (2008) Experimental and numerical investigation of the plunge stage in friction stir welding. J Mater Process Technol 203(1–3):411–419
104. Schmidt H, Hattel J (2004) A local model for the thermomechanical conditions in friction stir welding. Model Simul Mater Sci Eng 13(1):77
105. Guerdoux S, Fourment L (2009) A 3D numerical simulation of different phases of friction stir welding. Model Simul Mater Sci Eng 17(7):075001
106. Jedrasiak P, Shercliff HR, Reilly A, McShane GJ, Chen Y, Wang L, Robson J, Prangnell P (2016) Thermal modeling of Al-Al and Al-Steel friction stir spot welding. J Mater Eng Perform 25(9): 4089–4098
107. Heidarzadeh A, Jabbari M, Esmaily M (2015) Prediction of grain size and mechanical properties in friction stir welded pure copper joints using a thermal model. Int J Adv Manuf Technol 77(9–12): 1819–1829
108. Buffa G, Hua J, Shivpuri R, Fratini L (2006) A continuum based fem model for friction stir welding—model development. Mater Sci Eng A 419(1–2):389–396
109. Ulysse P (2002) Three-dimensional modeling of the friction stir-welding process. Int J Mach Tools Manuf 42(14):1549–1557
110. Colegrove PA, Shercliff H (2004) Development of Trivex friction stir welding tool part 2–three-dimensional flow modelling. Sci Technol Weld Join 9(4):352–361
111. Hossfeld M, Roos E (2013) A new approach to modelling friction stir welding using the CEL method, Advanced Manufacturing Engineering and Technologies NEWTECH 2013 Stockholm, Sweden 27–30 October 2013, p 179
112. Li K, Jarrar F, Sheikh-Ahmad J, Ozturk F (2017) Using coupled Eulerian Lagrangian formulation for accurate modeling of the friction stir welding process. Procedia Eng 207:574–579
113. Chu Q, Yang X, Li W, Vairis A, Wang W (2018) Numerical analysis of material flow in the probeless friction stir spot welding based on coupled Eulerian-Lagrangian approach. J Manuf Process 36:181–187
114. Pan W, Li D, Tartakovsky AM, Ahzi S, Khraisheh M, Khaleel M (2013) A new smoothed particle hydrodynamics non-Newtonian model for friction stir welding: process modeling and simulation of microstructure evolution in a magnesium alloy. Int J Plast 48: 189–204

115. Tartakovsky A, Grant G, Sun X, Khaleel M (2006) Modeling of friction stir welding (FSW) process with smooth particle hydrodynamics (SPH). SAE International, Warrendale
116. Yoshikawa G, Miyasaka F, Hirata Y, Katayama Y, Fuse T (2012) Development of numerical simulation model for FSW employing particle method. Sci Technol Weld Join 17(4):255–263
117. Padmanaban R, Kishore VR, Balusamy V (2014) Numerical simulation of temperature distribution and material flow during friction stir welding of dissimilar aluminum alloys. Procedia Eng 97: 854–863
118. Al-Badour F, Merah N, Shuaib A, Bazoune A (2014) Thermo-mechanical finite element model of friction stir welding of dissimilar alloys. Int J Adv Manuf Technol 72(5–8):607–617
119. Yaduwanshi D, Bag S, Pal S (2016) Numerical modeling and experimental investigation on plasma-assisted hybrid friction stir welding of dissimilar materials. Mater Des 92:166–183
120. Liu X, Lan S, Ni J (2015) Thermal mechanical modeling of the plunge stage during friction-stir welding of dissimilar Al 6061 to TRIP 780 steel. J Manuf Sci Eng 137(5):051017–051017
121. Liu X, Chen G, Ni J, Feng Z (2017) Computational fluid dynamics modeling on steady-state friction stir welding of aluminum alloy 6061 to TRIP steel. J Manuf Sci Eng 139(5):051004
122. Chen K, Liu X, Ni J (2017) Thermal-mechanical modeling on friction stir spot welding of dissimilar materials based on coupled Eulerian-Lagrangian approach. Int J Adv Manuf Technol 91(5–8): 1697–1707
123. Li K, Aidun D, Marzocca P (2009) Time-varying functionally graded material thermal modeling of friction stir welding joint of dissimilar metals. ASM International, Russell Township, pp 731–735
124. Torres E. CFD modelling of dissimilar aluminum-steel friction stir welds, Proc. 9th International Conference on Trends in Welding Research, A$M
125. Nandan R, Roy G, Lienert T, Debroy T (2007) Three-dimensional heat and material flow during friction stir welding of mild steel. Acta Mater 55(3):883–895
126. Arora A, Nandan R, Reynolds A, DebRoy T (2009) Torque, power requirement and stir zone geometry in friction stir welding through modeling and experiments. Scr Mater 60(1):13–16
127. Nandan R, Roy G, Debroy T (2006) Numerical simulation of three-dimensional heat transfer and plastic flow during friction stir welding. Metall Mater Trans A 37(4):1247–1259
128. Nandan R, Roy G, Lienert T, DebRoy T (2006) Numerical modelling of 3D plastic flow and heat transfer during friction stir welding of stainless steel. Sci Technol Weld Join 11(5):526–537
129. Chen K, Liu X, Ni J (2017) Keyhole refilled friction stir spot welding of aluminum alloy to advanced high strength steel. J Mater Process Technol 249:452–462
130. Liu X, Lan S, Ni J (2015) Electrically assisted friction stir welding for joining Al 6061 to TRIP 780 steel. J Mater Process Technol 219:112–123
131. Troitskii O, Likhtman V (1963) The anisotropy of the action of electron and radiation on the deformation of zinc single crystal in the brittle state. Kokl Akad Nauk 148:332–334
132. Ji S, Li Z, Wang Y, Ma L (2017) Joint formation and mechanical properties of back heating assisted friction stir welded Ti–6Al–4V alloy. Mater Des 113:37–46
133. Langenecker B (1966) Effects of ultrasound on deformation characteristics of metals. IEEE Transactions on Sonics and Ultrasonics 13(1):1–8
134. Ji S, Li Z, Ma L, Yue Y, Gao S (2016) Investigation of ultrasonic assisted friction stir spot welding of magnesium alloy to aluminum alloy. Strength Mater 48(1):2–7
135. Thomä M, Wagner G, Straß B, Wolter B, Benfer S, Fürbeth W (2018) Ultrasound enhanced friction stir welding of aluminum and steel: process and properties of EN AW 6061/DC04-Joints. J Mater Sci Technol 34(1):163–172
136. Liu X, Wu C (2015) Material flow in ultrasonic vibration enhanced friction stir welding. J Mater Process Technol 225:32–44
137. Curtis T, Widener C, West M, Jasthi B, Hovanski Y, Carlson B, Szymanski R, Bane W (2015) Friction stir scribe welding of dissimilar aluminum to steel lap joints. In: Friction stir welding and processing VIII. Springer, Berlin, pp 163–169
138. Jana S, Hovanski Y, Grant G, Mattlin K (2011) Effect of tool feature on the joint strength of dissimilar friction stir lap welds, Friction stir welding and processing VI, pp 205–211
139. Mofid M, Abdollah-Zadeh A, Ghaini FM (2012) The effect of water cooling during dissimilar friction stir welding of Al alloy to mg alloy. Mater Des (1980–2015) 36:161–167
140. Evans WT, Gibson BT, Reynolds JT, Strauss AM, Cook GE (2015) Friction stir extrusion: a new process for joining dissimilar materials. Manuf Lett 5:25–28
141. Reza E-Rabby M, Ross K, Whalen S, Hovanski Y, McDonnell M (2017) Solid-state joining of thick-section dissimilar materials using a new friction stir dovetailing (FSD) process, Friction Stir Welding and Processing IX. Springer, Berlin, pp 67–77